AN ABSTRACT OF THE THESIS OF

Anthonie Kramer for the degree of Master of Science in Civil Engineering and Wood Science presented on March 14, 2014.

Title: Cross-Laminated Timber Engineering: Improvement and Application

Abstract approved:

Andre R. Barbosa Arijit Sinha

The development of cross-laminated timber (CLT) panel technology has opened up new opportunities for wood in tall buildings. Several characteristics including seismic performance and speed of construction have raised interest among designers. As CLT gains acceptance in the industry, alternative structural solutions need to be investigated to improve performance of CLT as a building material. The first study presented is an assessment of the viability of hybrid poplar for use in CLT panels. Hybrid poplar is a low density species, which is not typically considered for structural applications. Low density species have the potential to improve the structural efficiency of CLT panels. The tests conducted are based on the qualification of panels outlined in the ANSI/APA PRG-320: Standard for Performance-Rated Cross-Laminated Timber to determine the structural viability of the CLT panels. The second study presented is an investigation of a new alternative energy dissipation solution to be used with cross-laminated timber rocking walls for seismic design. The energy dissipators are designed as a structural fuse which can be easily replaced after failure following a large seismic event. The results of this study give insight to alternative solutions for CLT to improve upon current applications.

Cross-Laminated Timber Engineering: Improvement and Application

by
Anthonie Kramer

A THESIS

submitted to

Oregon State University

in partial fulfillment of
the requirements for the
degree of

Master of Science

Presented March 14, 2014
Commencement June 2014

Master of Science thesis of Anthonie Kramer presented on March 14, 2014.

APPROVED:

Co-Major Professor, representing Civil Engineering

Co-Major Professor, representing Wood Science

Head of the School of Civil and Construction Engineering

Head of the Department of Wood Science and Engineering

Dean of the Graduate School

I understand that my thesis will become part of the permanent collection of Oregon State University libraries. My signature below authorizes release of my thesis to any reader upon request.

Anthonie Kramer, Author

ACKNOWLEDGEMENTS

I would like to express my gratitude for the guidance of my advisors Dr. Andre R. Barbosa and Dr. Arijit Sinha whose insight and support were essential to the success of the works presented here.

I would also like to thank the lab manager Milo Clauson for his mentorship over the past several years. He has taught me more than any engineering course could.

Last but not least I would like to thank my wife Kristine for her love and encouragement.

CONTRIBUTION OF AUTHORS

Dr. Andre R. Barbosa and Dr. Arijit Sinha reviewed and made revisions to the main text of both manuscripts. They also reviewed designs and assisted in the interpretation of data.

TABLE OF CONTENTS

TABLE OF CONTENTS (Continued)

Page

TABLE OF CONTENTS (Continued)

Page

LIST OF FIGURES

Figure Page

LIST OF TABLES

Table Page

LIST OF APPENDIX FIGURES

Figure Page

LIST OF APPENDIX FIGURES (Continued)

Figure Page

LIST OF APPENDIX TABLES

Table Page

CROSS-LAMINATED TIMBER ENGINEERING: IMPROVEMENT AND APPLICATION

1 General Introduction

1.1 Background

Cross-laminated timber (CLT) is amongst a latest line of engineered wood panels. CLT is a prefabricated solid engineered wood panel that was first designed in Austria in the mid-1990s and called Kreuzlagenholz (KLH). It was developed as a research project at the Graz University of Technology in Styria, Austria. This mass timber panel product is promoted as a sustainable alternative to steel or concrete systems, due to carbon sequestration. The majority of CLT projects in Europe have been in residential construction. Despite its increasing popularity over the past 20 years in Europe, it is only recently that CLT has made significant inroads in North America. Canada has led the research and development of CLT in North America, and the efforts have culminated in the form of the Canadian CLT Handbook (Gagnon and Pirvu 2011). With the publication of ANSI/APA PRG 320: Standard for Performance Rated Cross-Laminated Timber (2011) and then revised in 2012 (APA 2012), CLT has entered the mainstream construction material marketplace in the US. This standard has been approved by the Structural Committee of the International Code Council (ICC) for the 2015 International Building Code (IBC) in the U.S. to recognize CLT products as an acceptable construction material (Yeh et al. 2012).

Although CLT has gained recent approval into the IBC, misconceptions about the viability of mid-rise panelized timber buildings remain due to concerns regarding fire safety, durability, and seismic performance during large earthquake events. In Europe, standards for issues like fire protection and acoustics are being incorporated into building codes, and these have been discussed in recent literature in the construction of CLT mid-rise domestic buildings (Yates et al. 2008). Current manufacturing requirements limit CLT to dry service conditions which will prevent durability issues. Also, innovations in seismic design are creating new options for taller CLT structures (Ceccotti 2008). Furthermore, recent projects utilizing CLT as a primary structural material have shown

promising results. One example is Murray Grove Tower in London, UK which is built from CLT walls and floors. An advantage of CLT is the lack of pocket walls which would allow rapid spread of fire results in slow-burning construction (Langebach 2008). Murray Grove was one of the first projects to incorporate the use of CLT for mid-rise construction. The design investigation included the effect of creep, fire, and acoustic performance. CLT was shown to perform above the building code requirements in all of these areas. At nine stories tall, Murray Grove Tower whose construction was completed in 2009 was the tallest modern timber building in its time. This feat was only recently surpassed by the construction of the ten story Forte building in Melbourne, Australia in 2012 (Harris 2012). These projects, though impressive, are in regions with low to moderate seismic risk, which is the current threshold of CLT building design. Nonetheless, conceptual building solutions up to 30 stories that make use of CLT have been proposed in research (Green and Karsh 2012).

1.2 Cross-Laminated Timber Panels

CLT panel structural behavior is well understood, and the properties can be estimated using the shear analogy method (Kreuzinger 1999). The behavior of CLT panels depends on homogenization, and has been shown to have frequent rolling shear failures in bending tests (Steiger and Gulzow 2009). Due to the perpendicular orientation of layers, CLT has shown high variability in stiffness up to 20%. Current CLT technology is comprised of softwood species, typically using strength graded material. One limitation outlined in ANSI/APA PRG 320 is a minimum specific gravity of 0.35, which excludes the use of low-density woods. The potential benefits of using low-density woods in CLT include a lower seismic mass and opportunities for low cost species.

Two main tests are required for qualification according to ANSI/APA PRG. The first test is third-point bending (ASTM 2012) to determine the bending moment capacity and estimate the bending stiffness. The second is a short-span center point bending test (ASTM 2012) to determine the shear strength and interlaminar shear capacity. These tests are used to determine characteristic strength properties, which are useful in design. Adhesive specifications are outlined and must meet AITC 405 (ANSI 2008), for

structural grade adhesives. Low density species are generally not used with structural grade adhesives in a building material capacity and necessitate block shear tests to evaluate bond performance.

There is a need for researching alternate uses for low density species that is increasing from oversupply of typically nonstructural grade hardwoods. The use of woods such as hybrid poplar, which are grown on Forest Steward Council (FSC) certified sustainable timber plantations, gives a value-added use as a sustainable building material. This will be useful as CLT continues to gain acceptance in the industry.

1.3 Connection Systems

Investigation of CLT buildings under high seismic loading has been at the forefront of recent research. A seven-story CLT building was tested in 2007 on the world's largest earthquake shake table at the E-Defense research facility in Miki, Japan (Ceccotti et al. 2013). The building performance showed failures due to wall hold-down connections, with a ductile failure mode. High accelerations were observed, and it was noted that connections are critical to the behavior of the building. Connection design controls the hysteretic response of a building because of the strength and rigidity of CLT panels. The energy dissipation and ductility of the system is controlled by the connection system, due to the disparity in CLT panel and connection strengths (Lauriola et al. 2006). Additionally, joint layout influences the behavior of the structural system. Local failures in connections control the failure of the system, and axial stiffness and resistance is important (Gavric et al. 2011). Several tests have been performed on nail and screw based connections for CLT, which confirm the ductile local failure of connections and stress the importance of designing connections for overstrength to avoid brittle failure of the CLT panels at the toe of the wall (Ceccotti et al. 2006, Fragiacomo et al. 2011).

Models have been developed to predict the response of CLT buildings, and have successfully predicted hysteretic energy dissipation properties and seismic capacity reliably (Schneider et al. 2012, Rinaldin et al. 2013). CLT has been described as a predictable material in a building system that can be analyzed with basic computational

tools based on a seven-story model (Dujic et al. 2010). One particular barrier in CLT research has been the development of a seismic response modification factor (R). A recent study of mid-rise CLT buildings up to ten stories has resulted in an R value of 4.3 based on current connection systems (Pei et al. 2012). This takes into account the assumption that the connections allow the walls to rotate, and is valid for an inter-story drift up to 3%.

1.4 Advanced Connection Systems

Connection systems with high seismic performance have been developed and investigated largely in the past decade. One notable contribution was the development of post-tensioned rocking wall systems for precast concrete (Nakaki et al. 1999). These systems use an unbonded pre-stressing tendon to center the walls to minimize residual lateral displacement. This technique lacks adequate energy dissipation, which must be provided by additional dissipative connections. The structural solution that makes use of post-tensioned bars or cables and energy dissipation solutions are designated as hybrid self-centering systems or hybrid rocking systems. Development of energy dissipation solutions for hybrid rocking wall systems is a relatively new concept, particularly for use in timber structures. The only mass timber hybrid rocking wall solutions that currently exist are based on Laminated Veneer Lumber (LVL) beam-column connections and wall systems (Palermo et al. 2006). LVL performs similarly to CLT, and is useful for comparison. Enhanced performance from LVL hybrid connection systems was observed and provided high levels of ductility, negligible residual deformation, and no significant damage to structural elements. Full-scale tests were presented and pre-stressed systems were recommended for use in multi-story timber buildings due to re-centering behavior and adequate energy dissipation (Iqbal et al. 2010). Global response has also been investigated and produces excellent seismic behavior (Newcombe et al. 2010). These systems have been recently implemented in timber structures in New Zealand. These innovative structures ensure that the building will continue to function after a design level seismic event (Devereux et al. 2011). Hybrid rocking walls have also been implemented to minimize damage and promote sustainable building design through the use of timber

(Palermo et al. 2012). These projects employ the use of internal energy dissipators, which are difficult to replace following a large earthquake event.

Hybrid self-centering systems with external energy dissipators have been investigated with LVL, and have shown enhanced seismic performance (Smith et al. 2007). The external dissipators are sacrificial elements, and are designed to fail during a design earthquake. The attachment of energy dissipators is critical in ensuring rapid construction and ease of replacement after failure. The feasibility of self-centering timber structures has been studied and compared to steel and concrete construction. Post-tensioned hybrid timber structures are constructed quickly with minimal costs, and are comparable to steel and concrete options, providing a more sustainable alternative (Smith et al. 2008, Fragiacomo et al. 2009). After large seismic events, connections must be replaced, and design solutions need to explicitly address this design constraint. Herein lies the opportunity for this research.

1.5 Purpose of Study and Organization

The purpose of this study is to investigate potential improvements to CLT through new materials and technology. The specific objectives of the study are to:

1. Investigate the use of low-density species on CLT panels
2. Assess the viability of low-density species in meeting ANSI-approved CLT grades
3. Develop a new energy dissipation device that allows for enhanced and predictable seismic structural behavior
4. Investigate the potential for use of hybrid self-centering solutions in CLT walls

In order to fulfill these objectives two studies were undertaken, which resulted in two manuscripts. Supporting data and figures not included in the manuscripts are included in the Appendix. The first manuscript titled “Viability of Hybrid Poplar in ANSI Approved

Cross-Laminated Timber Applications" (Chapter 2) reports the results stemming from an investigation of hybrid poplar (Pacific Albus) and its structural properties and behavior when used in CLT panels. Use of hybrid poplar in CLT has two primary advantages. First, use of a low density material reduces the mass of panels, which could be beneficial for seismic applications, as well as providing better constructability. Second, hybrid poplar is a fast growing tree, and it was relatively inexpensive at the time of the study. The second manuscript titled "Design and Performance of Steel Energy Dissipators to be Used in Cross-Laminated Timber Self-Centering Systems" (Chapter 3) reports the investigation of external energy dissipators and the development of a connection system for use with CLT. The application is presented as an easily installed and replaced product, which minimizes costs associated with repair after large seismic events. A unique wall and floor connection system is designed for repeated use. The overall goal of these studies is to further CLT technology and to provide more efficient and cost effective solutions, which improve the feasibility of CLT tall building construction in regions of high seismic activity.

2 VIABILITY OF HYBRID POPLAR IN ANSI APPROVED CROSS-LAMINATED TIMBER APPLICATIONS

Anthonie Kramer, Andre R. Barbosa, and Arijit Sinha

Accepted for publication in

Journal of Materials in Civil Engineering

American Society of Civil Engineers

1801 Alexander Bell Drive, Reston, VA 20191-4400

DOI: 10.1061/(ASCE)MT.1943-5533.0000936

2.1 Abstract

The development of cross-laminated timber (CLT) technology has opened up new opportunities for low-density hardwood species, which have traditionally not been rated as construction-grade materials for structural engineering applications. Several characteristics of the CLT, namely thermal performance, seismic behavior, and speed of construction, have raised interest among designers. The CLT technology has recently been used for residential and non-residential multi-story buildings and it has been identified as one of the ways for achieving tall timber building construction. As CLT gains acceptance in the industry, low-density wood species, not specified in current American National Standards Institute (ANSI) standards, need to be investigated for potentially successful use in CLT panels. This paper presents a study that demonstrates the viability of a Forest Stewardship Council (FSC) certified sustainable plantation grown low-density species, hybrid poplar (marketed as Pacific Albus), for use in performance-rated CLT panels by following the ANSI/APA PRG-320-2012: Standard for Performance-Rated Cross-Laminated Timber shear and bending test guidelines to determine the structural viability of the CLT panels.

2.2 Introduction

Cross-laminated timber (CLT) is an engineered structural composite panel usually consisting of three to nine layers of dimensioned lumber arranged perpendicular to each other, much like layers of veneer in plywood. CLT has been successfully used as prefabricated walls, floor and roofing elements in residential, non-residential, and commercial structures, and is being proposed as a new solution for tall wood building construction (Mohammed et al. 2012). This is not only a new composite material but also a new building technology revolutionizing the use of timber in construction in a way not seen since the introduction of plywood as a structural-grade panel product. The CLT manufacturing process and the technology of erecting prefabricated houses based on this product have been developed in Europe over the last 15 years despite the lack of a European product standard. A European draft standard was published in 2011 (prEN16351 2011). In North America, the industry is still lagging behind their European

counterparts, and the recent efforts related to CLT have originated in Canada through an aggressive research program put forth by FP Innovations that led to the publication of a CLT Handbook (Gagnon and Pirvu 2011). Recognizing this gap in knowledge and in normative publications in the US, in 2011 the American National Standards Institute and the APA - The Engineered Wood Association published a standard for performance-rated CLT panels (ANSI/APA PRG 320), which was updated in 2012. This performance standard provides the requirements for the use of visually graded, machine stress rated, and structural composite lumber (SCL), in CLT panels. This standard proved to be an important first step towards acceptance of CLT in the US construction industry, as recently the International Code Council approved the inclusion of ANSI approved CLT panels as a building material in the International Building Code to be published in 2015 (AWC 2012). The US version of CLT handbook was released recently in February 2013.

The raw material most commonly used for construction of CLT in Europe is structural C24-grade spruce or pines, which have densities ranging from 420 kg/m^3 to 500 kg/m^3 at 12% moisture content (MC). In the US, the ANSI standard limits the use of lumber material to 350 kg/m^3 and above. As CLT gains acceptance in the industry, alternative and other low-density species of wood (not specified in ANSI/APA PRG 320), need to be investigated for potentially successful use in CLT panels.

The need for researching alternate uses for low-density species is increasing from oversupply of typically non-structural grade hardwoods. This is a challenge in the US, particularly with the reduction in demand for furniture manufacturing and pulp. Hybrid poplar is an example of low-density hardwood grown in the Pacific Northwest (PNW) region. The plantations were established to supply pulpwood to the PNW paper industry. Since the 1980's however, the pulp and paper industry in the PNW region has shrunk by half due to competition from overseas (Law 2011). Consequently, the plantation fiber is used mainly as biomass, pallets, and marginally in the furniture industry. The hybrid poplar plantations are Forest Steward Council (FSC) certified sustainable timber plantations. A value-added use for the wood is needed, preferably as a sustainable

building material. Hybrid poplar has shown excellent machinability characteristics as well as higher than average glue bonding strength (Carlson 1998).

The objective of this paper is to demonstrate the viability of FSC certified sustainable plantation grown low-density species, like hybrid poplar (density between 300-350 kg/m^3), for building structurally graded CLT panels. The viability of the low-density wood for use in CLT is based on a series of tests according to ANSI/APA PRG320-2011, namely by following shear and bending test guidelines to determine the characteristic strengths and stiffness of the panels.

2.3 Materials and Methods

2.3.1 Manufacturing of Cross-Laminated Timber

2.3.1.1 Species and Dimension of Wood

Hybrid poplar (marketed as Pacific Albus) was procured from Boardman, Oregon. The individual boards were No. 2 or better. The initial dimensions of the lumber were 36 x 140 x 3048 mm. The lumber was conditioned prior to CLT manufacturing in a standard room maintained at 20ºC and 65% relative humidity. The boards were planed prior to lamination. Additionally, each board was sized using a joiner in order to minimize gaps between boards created by minor warping. All of the CLT panels in these tests were three layered, each board averaging 32 mm in thickness, with each panel having a three board thickness totaling approximately 95 mm. The width of each board after sizing was approximately 135 mm, with each panel having three boards in width with an average full panel width of 410 mm after pressing. The lengths of the boards were cut to 2790 mm, in order to meet the necessary span-to-depth ratio of 27 required by the subsequent bending test method ASTM D4761 (ASTM 2012).

2.3.1.2 Adhesive Used

The adhesive used between the layers was Hexion CASCOPHEN® LT-5210J resin and CASCOSET® FM-6210 hardener (Hexion 1996). The adhesive was combined using

a resin-hardener mixture ratio of 2.5:1 (by weight). The resin is described as a liquid, phenol-resorcinol, timber laminating resin. The recommended spread for this adhesive was 55 to 100 pounds of mixed glue per 1,000 square feet of glue joint. The glue mixture for each panel was estimated using the recommended spread. This adhesive system is recommended for face laminating softwoods for wet-use or dry-use exposure and meets the requirements of ANSI/AITC A190.1-02 (AITC 1992) and also conforms to AITC 405 (ANSI 2008).

2.3.1.3 Description of the Pressing Process

Developing a pressing process required some ingenuity. The recommended pressure for the adhesive was 700 to 1000 kPa. With a panel width of 410 mm and a panel length of 2540 mm, the total lamination area was approximately 1.05 square meters, which required a minimum force of 735 kN to reach target pressure. This was accomplished through a system of 8 threaded rods (38 mm) and nuts, which carried the load through a configuration of multiple 6.4 mm steel c-channels (Fig. 2.1).

Fig. 2.1. Fixture for pressing CLT panels

The applied wrench torque, T, in each nut was 700 N-m, which converted to 123 kN of preload force F_i per rod i. This conversion is based on the following formula:

$$T = KF_i d \quad (1)$$

where, d is the diameter of the bolt, and K is the correction factor taken as 0.15 for lubricated bolts. The maximum calculated force on the panel is approximately 985 kN, which meets the pressing requirement for the adhesive being used.

The panel layup was random with regard to the consideration of the placement and orientation of individual boards. The adhesive mixture was applied using a paint roller. The total assembly time of each test specimen was less than 60 min, measured from initial mixture to total pressure applied to final layup. The required pressing time for the adhesive was approximately 8 hours, which was always met or exceeded.

2.3.1.4 Final Specimen Preparation

Due to irregularities in individual boards, dimensions of the final panels varied slightly, and these were re-cut to ensure straight edges. This was accomplished using a large band saw. The average value for panel width after cutting was 400 mm. Samples were also finely sanded in areas where Digital Image Correlation (DIC) techniques were used, in order to establish a smooth surface, which minimized errors in the DIC measurements.

2.3.2 Testing Methods

2.3.2.1 Non-Destructive Bending Tests

There were 10 individual boards that made up each CLT panel, and each board was tested for dynamic modulus using a Metriguard Model 340 E-Computer, and a transverse vibration method to obtain the dynamic modulus of elasticity, that was averaged and reported in Table 2.1 as Average Board Modulus of Elasticity (ABMOE), as well as specific gravity (SG). The results from the CLT panels were compared to their constituents to verify a correlation between individual board stiffness and panel stiffness. These tests were completed on all of the boards, except for the boards used to

manufacture the first panel, since a correlation between individual board strength and panel strength was not considered until the results from the first panel were compared with published hybrid poplar properties.

Table 2.1: Results from bending tests

Test	MOR	MOE	ABMOE	Maximum Load	Deflection at Failure	SG
Units	MPa	MPa	MPa	kN	mm	-
01	17	7202	-	26	35	-
02	23	7050	9239	34	48	0.367
03	29	8291	8308	42	60	0.348
04*	-	7288	8042	-	-	0.345
05*	-	7443	7577	-	-	0.344
06	25	7120	7776	37	54	0.341
07	34	7097	7909	50	65	0.338
Mean	26	7356	8142	38	52	0.347
STDEV	6	433	591	9	12	0.010
COV	24.9%	5.9%	7.3%	24.2%	22.4%	3.0%
Legend	MOE - Apparent Modulus of Elasticity (adjusted with composite factor k) ABMOE - Average Board Modulus of Elasticity (dynamic, adjusted with composite factor k for comparison) SG - Specific Gravity (measured dynamically) STDEV - Standard Deviation COV - Coefficient of Variation *Panels not tested to failure; cut into sections for short span tests					

2.3.2.2 Bending Tests

There are a number of ways to assess bending properties for a panel. The method found to be most suitable for this study was ASTM D4761 (ASTM 2012) for bending flatwise third point loading as recommended in ANSI/APA PRG 320 (APA 2012). The testing apparatus used is shown in Fig. 2.2.

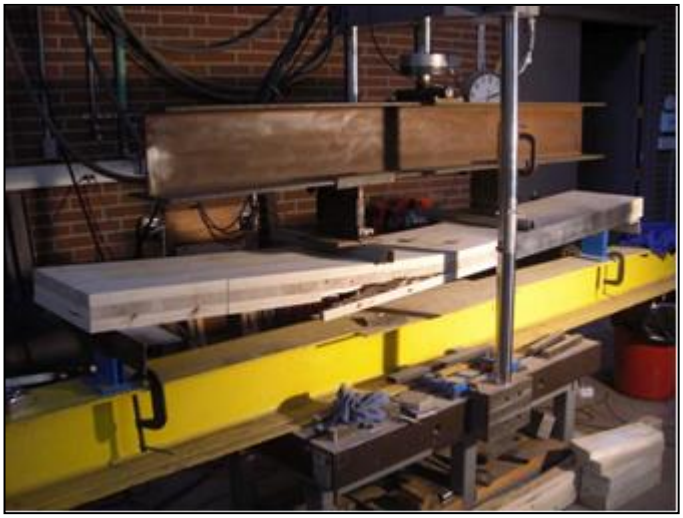

Fig. 2.2. Test set up and a panel (06) at failure and equations for calculating modulus of elasticity and modulus of rupture

Specimen thickness was approximately 95 mm, therefore on-center span of 2.54 meters was used to achieve an approximate span-to-depth ratio of 27. Specimen width was an average of 400 mm.

The loading rate used was approximately 12.7 mm per minute, which gave an adequate time of 3 to 5 min to reach failure as required by ASTM D4761. Load was applied using a MTS actuator with 178 kN load capacity and a 250 mm stroke length. A LVDT sensor was used at the center-line to obtain deflection. A load-deflection curve was hence obtained and used for calculating the measured modulus of elasticity (MOE). The MOE calculated was the apparent modulus of elasticity, which is given in Eq. 2 (ASTM 2009). The modulus of rupture (MOR) was calculated using Eq. 3.

$$MOE = \frac{23PL^2}{108bh^2\Delta} \tag{2}$$

$$MOR = \frac{P_{\max}L}{bh^2} \tag{3}$$

where, P is the applied load (N); L is the span of the CLT (mm); b is the width (mm); h is the depth of CLT (mm); Δ is center-span deflection measured from the LVDT (mm); and P_{max} is the maximum applied load.

The values from Eqs. 2 and 3 do not take into account adjustments for composite sections, so an adjustment was made using the k-method of composite theory (Blass and Fellmoser 2004). For a three layer section, the equation is:

$$k = 1 - \left(1 - \frac{E_{90}}{E_0}\right)\left(\frac{a_{m-2}^2}{a_m^2}\right) \tag{4}$$

where, k is the composite factor, E0 is the MOE in the longitudinal direction, E90 is the MOE in the transverse direction, a_{m-2} is the thickness of the inner layer, and a_m is the outside (total thickness) of the section. Using the general assumption from the CLT Handbook that E90 = E0 / 30, the equation further simplifies to:

$$k = 1 - \left(1 - \frac{29}{30}\right)\left(\frac{a_{m-2}^2}{a_m^2}\right) \tag{5}$$

Since all specimens in this test are approximately the same size and configuration, the composite factor k is computed using Eq. 5 (with a_{m-2} = 32mm and a_m = 96mm) which equates to 0.964 for all panels. This factor is applied to all MOE and MOR values obtained using Eq. 2 and 3 respectively, since Eqs. 2 and 3 are for beams with solid rectangular homogeneous cross-sections.

During the bending tests, an optical measurement instrument based on the principles of Digital Image Correlation (DIC) was used to measure the strain that developed on the x-z plane along the edge of the panels. DIC is a full- field, non-contact technique for measurement of displacements and strains. The principle behind DIC is well understood and its application for shear wall assemblies has been previously demonstrated successfully by Sinha and Gupta (2009). The DIC setup consisted of a pair

of cameras arranged at an angle to take stereoscopic images of the area of interest. The area of interest was adjacent to the loading point, where the largest combination of shear and bending moment were expected. Once the cameras were set up for each test, a calibration of the DIC system was done to reduce error in the measurements. The cameras were externally triggered to capture images at a rate of one picture every ten seconds during the tests and were connected to a computer where the images are stored. Using Vic 3D (Correlated Solutions Inc., 2010), the images were analyzed to obtain strain values for the areas of interest.

2.3.2.3 Short Span Bending Tests

Short span bending tests were conducted according to ANSI/APA PRG-320 (APA 2012), which refers back to the center point tests described in ASTM D4761 (ASTM 2012). These tests were used to determine the maximum shear stress (f_v) and the interlaminar shear capacity (f_s). The testing equipment was the same as used in the third point bending tests. These short span tests had a span of 510 mm, which is approximately 5 to 6 times the depth (95 mm). The overhang to either side of the supports was minimal. The loading rate of 1.27 mm/min ensured that the tests met the minimum requirement of 4 min to reach failure.

2.3.2.4 Block Shear Tests

Block shear tests were conducted according to ASTM D905 (ASTM 2012), at a loading rate of 5 mm/min in a universal testing machine with 100 kN (22.5 kips) capacity. Specimens were prepared according to the ANSI standard. Load was applied to the side of the sample that had a parallel grain direction, leaving the bearing side to the perpendicular grain section. The results from this test are considered to provide only an approximation of the shear strength, since there is not enough data to support a precise method to obtain the shear capacity of the given configuration.

2.4 Results and Discussion

2.4.1 Non-Destructive Bending Test

The values obtained from the non-destructive bending tests represent the dynamic modulus of elasticity. The mean value for these tests was 8450 MPa, which is slightly higher than the anticipated value when compared to a similar hybrid specimen static bending MOE value of 7540 MPa (Hernandez et al. 1998). Transverse vibration estimates of dynamic MOE have been known to overestimate the static bending MOE by 4-5% in Douglas-Fir samples (Ross et al. 2005), which may explain the higher values obtained. The actual difference in this study estimates the dynamic modulus as approximately 11% higher after adjusting for composite section values in both the static CLT panel tests and individual board tests. This is reasonable considering the relatively small sample size, which affects the accuracy of this study.

2.4.2 Bending Tests, Strain Progression, and Failure Mechanisms

The results from the third point bending tests are presented in Table 2.1, which includes MOR, apparent MOE, failure load, and deflection. All seven panels were tested for MOE, with panels 04 and 05 not tested to failure, in order to obtain short span test specimens. The mean MOR was 26 MPa with a COV of 25%, which is relatively high for a wood composite. Smaller sample size (5 panels) and laboratory manufacturing procedures might have led to larger variability. The mean apparent MOE was 7360 MPa, with a COV of 5.9%. Higher variation is observed in strip shaped specimens such as the ones in this study compared to full sized panels (Steiger and Gulzow, 2009) due to the heterogeneous nature of the material. Comparing the adjusted MOE values for the panel to another hybrid poplar specimen, the mean result was only 2% lower than Hernandez et al. (1998).

The values calculated for this study were a ranked percentile with linear interpolation between closest ranks, which gives a 5^{th} percentile value using the range of values within a sample set. These values were calculated only for comparison purposes with the ANSI standard. No attempt was made to establish design parameters for CLT manufactured

with hybrid poplar. The 5th percentile MOE was 7100 MPa while MOR was 18.2 MPa. Comparison of these values to the characteristic values in ANSI/APA PRG 320 (APA 2012) shows that the MOE obtained experimentally is lower than the MOE of the lowest CLT Grade E3 (MOE = 8300 MPa). On the other hand, characteristic MOR values observed were higher than the listed values for Grade E3 (17.4 MPa). This indicates a potential for hybrid poplar to meet the bending strength requirements of CLT Grade E3, but not meet the current ANSI/APA PRG 320 (APA 2012) MOE requirements, which is expected since hybrid poplar is a low-density wood species with a lower MOE.

Fig. 2.2 illustrates the commonly observed failure mechanism. Most of the panels (Tests 02, 03, 06, 07) failed in combined bending and shear in the region located next to the loading points in the section closest to the supports. DIC measurements were taken in several specimens tested in bending and an example of strain distribution (Test #06) throughout the composite section is presented in Fig. 2.3.

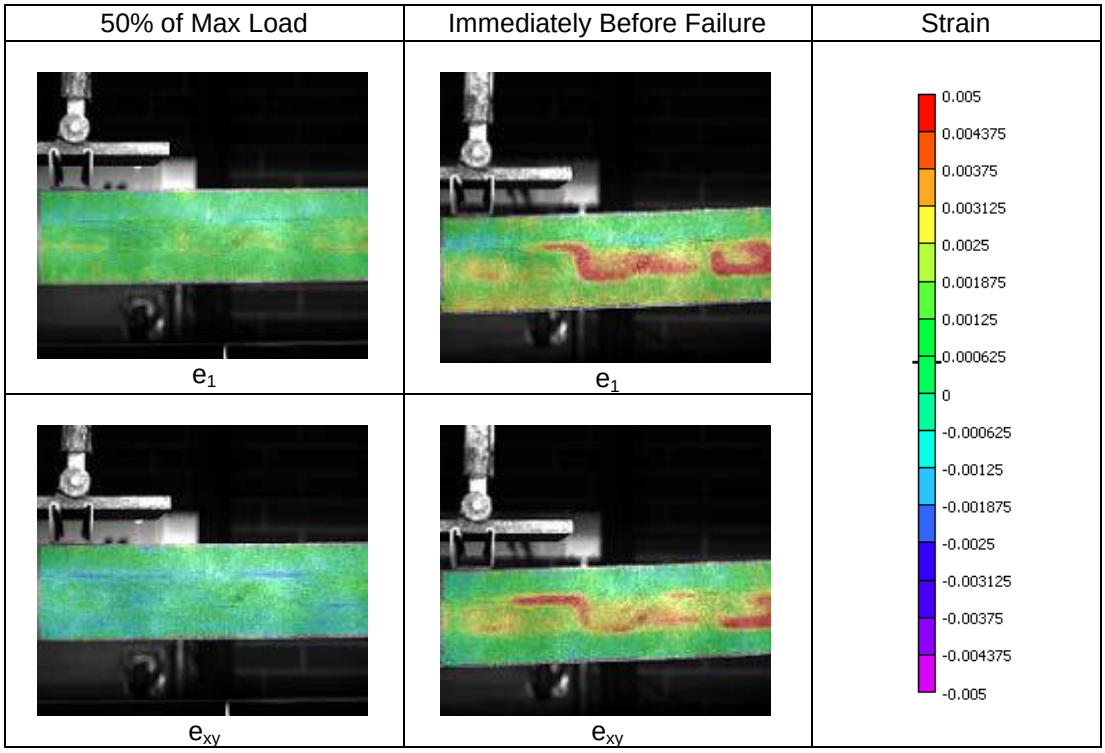

Fig. 2.3. DIC strain measurement at 50% max load and immediately before failure along with its legend

The DIC images (Fig. 2.3) are taken at 50% of maximum load and immediately before failure of the specimen. As expected, the maximum longitudinal strains are seen at the top and bottom of the section due to bending. It should be noted that the boards were not edge glued, which may have contributed to the large amount of strain in the middle section shown in e_1 (major principal) strain immediately before failure. The shear strain (e_{xy}) contour plot in Fig. 2.3 provided an indication of the typical failure path, which can be seen in Fig. 2.2. The strain progression is assumed to be nearly symmetric across the centerline up to failure. It is further observed that the strain in the section tends to concentrate both in the laminations between the layers and the edges of the center layer boards. Strain is greatest between the loading point and the support, following a diagonal path along the top lamination, through a center layer board edge, and along the bottom lamination. The maximum strains occurred along the typical failure path, which is a

diagonal cracking that develops near the loading point at the top to a point closer to the support at the bottom.

2.4.3 Short Span Bending Tests and Failure Mechanisms

Short span bending tests provided maximum shear stress (f_v). This in turn was used to estimate the interlaminar shear capacity (f_s) based on one third of the calculated f_v. The COV associated with shear stress was 15% (Table 2.2), which is comparable to other similar wood products.

Table 2.2: Results from short span bending and block shear tests along with their standard deviations (STDEV) and coefficient of variations (COV)

Short Span Bending Tests					**Block Shear Tests**		
Test	**Modulus of Rupture**	**Max Shear Stress**	**Max Load**	**Failure Deflection**	**Test**	**Max Load**	**Shear Strength**
Units	MPa	MPa	kN	mm	Units	kN	MPa
04 - 01	24.0	2.08	115	15.3	01 - B2	6.67	3.50
04 - 02	20.1	1.76	98.0	13.0	01 - B3	5.75	2.85
04 - 03	17.2	1.50	83.0	8.70	02 - B1	5.82	2.93
04 - 04	26.0	2.27	125	13.9	02 - B2	5.56	2.81
05 - 01	28.2	2.45	134	13.5	02 - B3	6.26	3.16
05 - 02	22.9	1.99	110	13.2	03 - B1	6.33	3.14
05 - 03	21.2	1.84	102	8.40	03 - B2	6.53	3.28
05 - 04	24.6	2.14	118	11.2	03 - B3	5.57	2.80
Mean	23.0	2.00	111	12.1	Mean	6.06	3.06
STDEV	3.00	3.02	16.0	2.50	STDEV	0.44	0.25
COV	15.1%	15.1%	14.7%	20.4%	COV	7.20%	8.20%

Failure during short span tests was similar to failure observed in the long span bending tests. Typical failure was in shear adjacent to the loading point, carried from the bottom layer near the supports, to the top layer near the loading point. Additionally, few tests exhibited small tension cracks that developed in the bottom layer directly below the loading point. Shear throughout the section was the primary failure mechanism in the

short span bending tests. The ranked 5th percentile values, which were calculated for comparison purposes only, were a shear capacity f_v = 1.6 MPa, with a corresponding interlaminar shear capacity f_s = 0.53 MPa. The characteristic test values from ANSI/APA PRG-320 for CLT Grade E3 are f_v = 1.3 MPa, and f_s = 0.43 MPa. Therefore, hybrid poplar potentially meets the ANSI/APA PRG-320 shear strength requirements.

2.4.4 Block Shear Tests

The shear strength values obtained from the block shear tests (Table 2.2) were greater than the shear strength values obtained from the short span bending tests. Additionally, a relatively low COV of 8.2% was observed (Table 2.2). Shear strength values from ASTM shear block tests tend to overestimate the failure shear stress from bending tests in structural composite lumber (Lam and Craig 2000). Wood failure in excess of 85% was observed in all samples, which suggests good adhesive bonding (AITC 2007). During testing, some squashing occurred in the bearing side of the block that had a grain orientation perpendicular to the loading plane. This may have affected some of the test values of the shear strength. Since there are no active standards that address the orthogonal layering configuration of CLT, this method is an approximation due to possible variation from rolling shear, which is the shear through the wood rather than the adhesive. The orientation of CLT should be considered when looking at strength results and evaluating adhesives. Block shear methods could be useful in the future to estimate shear strength without having to perform full panel testing.

2.5 Conclusion and Recommendations

The practical implication of the testing program performed was to determine whether hybrid poplar is a viable option for use in structural design of CLT. The results from the long and short span bending tests are promising since the experimental results show that the low-density (hybrid poplar) CLT will potentially meet and exceed the shear and bending strength requirements for ANSI/APA PRG-320 CLT Grade E3. However, hybrid poplar did not meet the stiffness requirements (MOE). These strength and stiffness testing results show that hybrid poplar CLT panels have a high structural efficiency (ratio

between mechanical performance and wood density) and indicate that structural design using low-density CLT panels would be governed by deflection. It is worth noting that hybrid poplar has not traditionally been used for structural applications, and emphasis should be placed upon accurate grading of boards and attention given to their location during panel layup.

Design of wooden structures is largely dictated by serviceability requirements. Although there are many current applications where CLT panels are used effectively, the use of hybrid poplar in CLT may not meet serviceability conditions on its own. However, like other engineered wood products, hybrid poplar could be utilized in conjunction with higher density species to achieve more efficient panels. More research is needed on CLT panels comprised of multi-species layers including low-density species such as hybrid poplar.

The work presented herein is a first step that provides encouraging results in what concerns the use of hybrid poplar for structural applications. Nonetheless, in the future, a testing campaign that includes a larger number of samples should be undertaken to optimize the layering scheme of the hybrid poplar CLT panels. Furthermore, development of design guidelines and analysis verification tools can be developed to improve dissemination of the proposed CLT panel solution.

2.6 Acknowledgements

The authors would like to thank Milo Clauson for his technical assistance in the laboratory. The authors would also like to acknowledge the help and support of Dr. Lech Muszynski.

2.7 References

American Institute of Timber Construction (AITC). (2007), "Test Methods for Structural Glued Laminated Timber." *AITC T107.* Centennial, CO.

American Institute of Timber Construction (AITC). (1992), "Structural Glued Laminated Timber." *ANSI/AITC A190.1-02.* Centennial, CO.

American National Standards Institute (ANSI). (2008). "Standard for adhesives for use in structural glued laminated timber." *ANSI 405-2008.* New York, NY.

American Society for Testing and Materials (ASTM). (2009), "Standard Test Methods of Static Tests of Lumber in Structural Sizes." *ASTM D198-09. Annual Book of ASTM Standards, Vol. 04.10. ASTM.* West Conshohoken, PA.

American Society for Testing and Materials (ASTM). (2012), "Standard Practice for Evaluating Allowable Properties for Grades of Structural Lumber." *ASTM D2915 – 03. Annual Book of ASTM Standards, Vol. 04.10. ASTM.* West Conshohoken, PA.

American Society for Testing and Materials (ASTM). (2012), "Standard Test Method for Strength Properties of Adhesive Bonds in Shear by Compression Loading." *ASTM 905-08. Annual Book of ASTM Standards. Vol. 15.06. ASTM.* West Conshohoken, PA.

American Society for Testing and Materials (ASTM). (2012), "Standard Test Methods for Mechanical Properties of Lumber and Wood-Base Structural Material." *ASTM D4761-05. Annual Book of ASTM Standards, Vol. 04.10. ASTM.* West Conshohoken, PA.

APA -The Engineered Wood Association. (2012), "Standard for Performance-Rated Cross-Laminated Timber." *ANSI/APA PRG 320.* Tacoma, WA.

Blass, H. J., & Fellmoser, P. (2004). "Design of solid wood panels with cross layers." *8th World Conference on Timber Engineering,* 14(17.6).

Carlson, M. (1998). "Solid Wood Products Opportunities from Short Rotation Hybrid Poplar Trees." *Science Council of BC.*

Correlated Solutions, Inc., 121 Dutchman Blvd, Columbia, SC 29063

Gagnon, S. and Pirvu, C., Eds. (2011). "CLT Handbook: Cross-Laminated Timber." *FPInnovations.* Vancouver, BC, Canada.

Green D.W., Winandy J. E., and Kretschmann, D.E. (1999). "Mechanical Properties of Wood. Wood Handbook: Wood as an Engineering Material" *General Technical Report FPL-GTR-190.* Department of Agriculture, Forest Service, Forest Products Laboratory. Madison, WI.

Hernández, R. E., Koubaa, A., Beaudoin, M., and Fortin, Y. (1998). "Selected Mechanical Properties of Fast-growing Poplar Hybrid Clones." *Wood and Fiber Science.* 30(2), 138–147.

Hexion Specialty Chemicals, Inc., (1996). "CASCOPHEN® LT-5210J Resin and CASCOSET® FM-6210 or FM-6210(S) Phenol-Resorcinol Adhesive System." <http://www.hexitherm.com/pdf/LT-5210J_FM-6210(S).pdf> (June 16, 2012).

Jones, F. D., Oberg, E., and Horton, H. L. (2004). *Machinery's handbook.* Industrial Press, Incorporated.

Lam, F. and Craig, B.A. (2000). "Shear Strength in Structural Composite Lumber." *Journal of Materials in Civil Engineering,* 12 (3), 196–204.

Law, S. (2011). "A crumpling paper industry. Once-mighty Oregon industry losing to mills overseas." *The Portland Tribune (online issue).* Portland, OR.

Mohammad, M., Gagnon, S., Douglas, B.K., and Podesto, L. (2012). "Introduction to cross laminated timber." *Wood Design Focus,* 22(2), 3-12.

Okkonen, E. A., and River, B.H. (1989). "Factors Affecting the Strength of Block-shear Specimens." Forest Products Journal. 39 (1): 43.

prEN16351 (2011). "Timber Structures - Cross Laminated Timber – Requirements." *European Standard, CEN.*

Ross, R. J., Zerbe, J. I., Wang, X. , Green, D. W., and Pellerin, R. F. (2005). "Stress Wave Nondestructive Evaluation of Douglas-fir Peeler Cores." *Forest Products Journal,* 55 (3), 90–94.

Sinha, A., and Gupta, R. (2009). "Strain distribution in OSB and GWB in wood-frame shear walls." Journal of Structural Engineering, 135(6), 666–675.

Steiger, R., and Gülzow, A. (2009). "Validity of Bending Tests on Strip-shaped Specimens to Derive Bending Strength and Stiffness Properties of Cross-laminated Solid Timber (X-lam)." *Proceedings of CIB-W18 Timber Engineering,* Karlsruhe, Germany. 42–12.

3 DESIGN AND PERFORMANCE OF STEEL ENERGY DISSIPATORS TO BE USED IN CROSS-LAMINATED TIMBER SELF-CENTERING SYSTEMS

Anthonie Kramer, Andre R. Barbosa, and Arijit Sinha

Journal of Structural Engineering

American Society of Civil Engineers

1801 Alexander Bell Drive, Reston, VA 20191-4400

Prepared for Submission

3.1 Abstract

This paper presents a new alternative energy dissipation solution to be used with cross-laminated timber (CLT) self-centering walls. CLT is a relatively new building product in North America, and could potentially be used for high-rise construction. The development of high performance seismic design solutions is necessary to encourage innovative structures. The objective of this study is to investigate a connection system that is easy to install and replace (structural fuse), and designed to be used with a self-centering CLT rocking wall. The proposed energy dissipators are fabricated following concepts used in developing steel Buckling Restrained Braces (BRB), having a milled portion which is designed to yield and is enclosed within a grouted steel pipe. The connection system is investigated experimentally through a unique test sequence of displacement-controlled cycles based on a modified version of the test method developed by the American Concrete Institute (ACI) to facilitate development of special precast systems [ACI T1.1-01 Acceptance Criteria for Moment Frames Based on Structural Testing]. Digital Image Correlation (DIC) was used to analyze strain behavior of the milled portion, as well as track movement of the panels during quasi-static uniaxial and cyclic testing. The results show the energy dissipation properties of the connection system. Damage was focused primarily in the energy dissipators, with negligible deformation and damage to the CLT panels and connections. These tests demonstrate the ability of these systems to be used as a viable energy dissipating solution in self-centering rocking or hybrid systems.

3.2 Introduction

Cross-laminated timber (CLT) buildings have previously demonstrated potential use in seismic zones for mid-rise construction through full-scale seven-story shake table tests at Japan's E-Defense facility in Miki, Japan (Ceccotti et al. 2013). Self-centering rocking systems have been presented as a high-performance seismic design solution to reduce residual drift after a large magnitude earthquake event, and have been demonstrated for precast concrete walls (Rahman and Restrepo 2000). These systems have an unbonded post-tensioning cable and are typically used with rigid wall panels which are allowed to

rotate. Vertical unbonded post-tensioning cables are used as a re-centering mechanism, and alone contribute negligibly to the total inelastic energy dissipation (Kurama et al. 1999). This has led to the development of hybrid self-centering rocking systems, which incorporate internal energy dissipators to increase the lateral load capacity and reduce lateral drift (Kurama 2000, Holden 2003). Hybrid systems produce a flag-shaped hysteretic response controlled through design of the post-tensioning and energy dissipators, which affects the equivalent viscous damping of the system (Restrepo and Rahman 2007). Steel energy dissipators are designed to yield during a large earthquake event, but must be replaced afterwards; leading to potentially expensive maintenance costs for systems with internal dissipators or welded steel connections.

Externally mounted dissipators have been successfully proposed for use in new design and retrofit for precast concrete assemblies (Marriott et al. 2008, Marriott et al. 2009, Rahman and Restrepo 2000). The latter used Buckling-Restrained Fuse-type (BRF) mild steel dissipators which were rigidly fixed to the specimens or testing apparatus (Sarti et al. 2013). Similar systems have also been successfully tested for Laminated Veneer Lumber (LVL) assemblies (Smith et al. 2007), which is a functionally similar structural system to CLT. This research has led to recent implementation of LVL hybrid rocking wall systems for high seismic performance timber buildings in New Zealand (Devereux et al. 2011, Palermo et al. 2012). To date, similar applications using CLT wall systems have not been proposed.

The objective of this study is to propose and evaluate the performance of an inexpensive energy dissipative solution that is easy to install and replace to be used in as part of a hybrid rocking wall system. Steel energy dissipators have previously shown undesirable behavior such as buckling, which may be initiated by rigid connections inducing a bending moment during panel rotation (Guerrini et al. 2012). This study presents a novel approach using a pinned end connection system, intended to allow rotation at the ends of the energy dissipators to reduce internal moments. The tensile behavior was studied due to the onset of buckling, which is strongly dependent on the maximum value of the tensile strain reached before the reversal (Rodriguez et al. 1999).

Additionally, the connections were designed to allow for quick swapping of energy dissipators after a large earthquake event.

The experimental program presented here consists of three individual tension tests, three panel tension tests including the connection system, and five panel cyclic tests. The experimental program was designed to verify the steel energy dissipator properties and the behavior of the connection system, including the local strain behavior of the milled section, which is tracked in tension testing using Digital Image Correlation (DIC) techniques. The latter quasi-static cyclic (reversed) tests were conducted according to a modified version of ACI T1.1-01 (ACI 2001), which is the criterion used previously for qualifying hybrid precast and LVL rocking wall systems. The modification is to keep the energy dissipator in the tensile strain range, which is the idealized case due to the orientation of the energy dissipator on the CLT panel. The rocking behavior of the wall panel is assumed to only cause uplift at the location of the energy dissipator. The results show that there are tolerances in the system from pinned and bolted connections. The local strain behavior is analyzed to better understand how buckling mechanisms manifest. Two prototype energy dissipator designs are presented, the second of which is a revision on the first to delay onset of buckling.

3.3 Experimental Design

Energy dissipator design depends on several factors. When considering the milled section, the design drift and geometry of the wall panel are the primary factors. The energy dissipators for our experiments were designed based on a 3.5% lateral drift to meet the requirements of ACI T1.1-01. The geometry is detailed in Fig. 3.1.

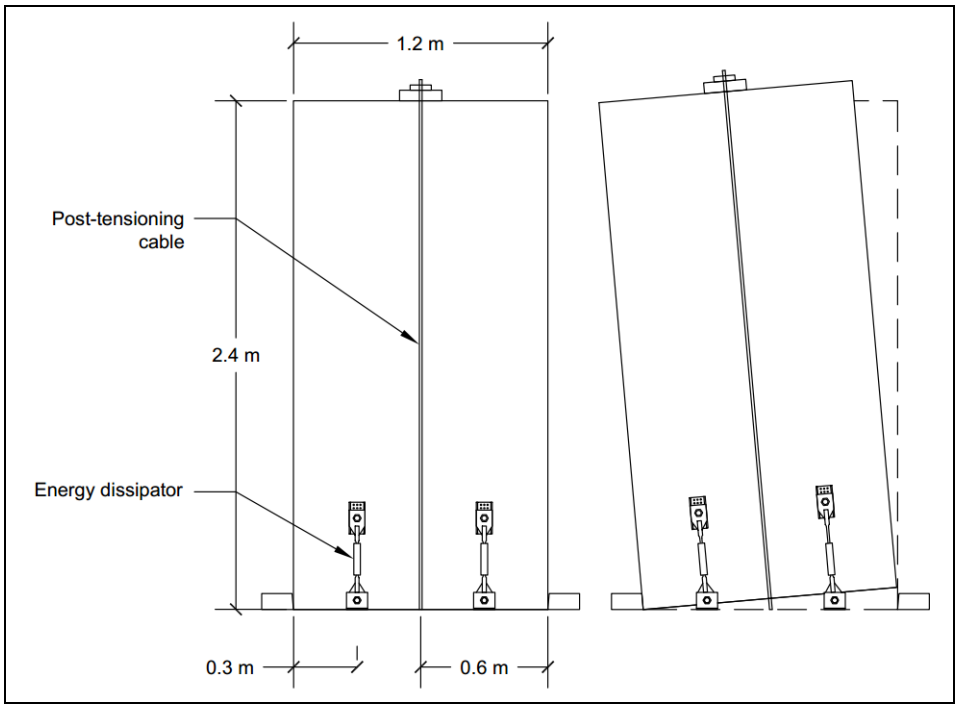

Fig. 3.1. CLT rocking wall assembly geometry

When the wall rotates, the uplift at the energy dissipators is 1/8 and 3/8 of the lateral drift (Fig. 3.1). For this wall assembly, a 3.5% drift is equal to approximately 85 mm lateral displacement, and a maximum of 32 mm of uplift at the energy dissipators. The dissipators were designed to reach ultimate strength, occurring at 20% strain in mild steel. The design resulted in a milled section length of approximately 152 mm. The milled section is a smaller diameter portion in the middle of the energy dissipator that is designed to yield.

To overcome the force required to return the energy dissipator to its original position after plastic deformation, a re-centering factor (λ) of approximately 1.25 was used as recommended (Palermo et al. 2007). The equation for λ can be seen in equation 1.

$$\lambda = \frac{M_{pt} + M_N}{M_s} \tag{1}$$

Where, M_s is the moment contribution from the energy-dissipating reinforcement, M_{pt} is the moment provided by the unbonded post-tensioning, and M_N is the moment provided by axial load including self-weight. After choosing a 9.5 mm diameter milled section for the energy dissipator, a single seven wire pre-stressing strand of 15 mm diameter would need to be used for a full wall test based on λ. The capacity of the energy dissipators was used to design the connection system to the wall panel and floor.

The connections were designed using procedures in the National Design Specification (NDS) for Timber Construction. For brevity, details of the design are excluded here, but can be found in the appendix. The connection system was designed to function as a low profile solution that would be relatively easy to cover up in a building. The design is an easy to install system that would be durable enough for re-use, allowing for rapid change out of energy dissipators after an event. Bending of the ends was a concern based on previous work (Guerrini et al. 2012), which influenced the pin ended dissipators adopted here, since these prevent bending stresses in the connection. A 3-D rendering of the connection system and the energy dissipator can be seen in Fig. 3.2. The connection consists of: (1) the wall panel connection, (2) the energy dissipator, (3) a 25.4 mm (nominal) diameter 415 MPa strength threaded rod, (4) bolted floor connection, and (5) a 25.4 mm (nominal) diameter 415 MPa strength bolt.

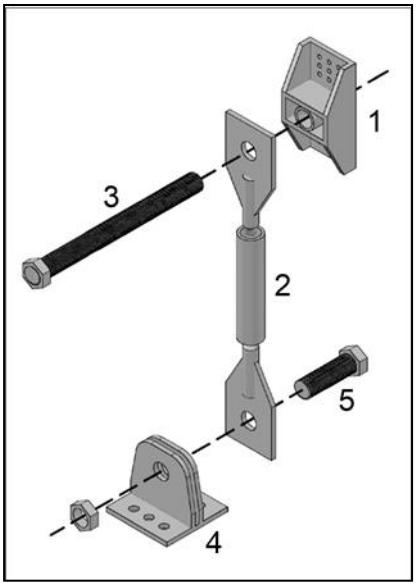

Fig. 3.2. Connection system

3.4 Materials

3.4.1 Cross-Laminated Timber

The CLT panels consisted of no. 2 and better, kiln dried Douglas-fir. Boards were nominal 2x6 (38 mm x 140 mm) and planed prior to adhesive application. The adhesive used was HexiTHERM® CASCOPHEN® LT-5210J resin with CASCOSET® FM-7400 hardener. The panels were pressed at approximately 1 MPa using a floor clamping system that was described in Chapter 2. At the time of pressing, the Douglas-fir had an average moisture content of 11% estimated with a moisture meter, which met the requirement of the adhesive. The final dimensions of the test panels were 600 mm x 600 mm x 150 mm.

3.4.2 Steel Energy Dissipators

The energy dissipators were made from hot rolled A36 steel. They were comprised of 6.4 mm flat bar, 19.1 mm round bar, and 25.4 mm diameter schedule 40 steel pipe; these made up the flanges, milled section, and outside sleeve, respectively. Flanges were arc welded to the shoulders of the milled section. To prevent buckling of the milled section, the sleeves were filled with BASF Embeco 885 grout, which has been shown to perform well under dynamic loading (Guerrini et al. 2012).

3.4.3 Wall and Floor Connections

The connections to the panel were made from hot rolled A36 steel, and were comprised of 6.4 mm flat bar. These were arc welded during fabrication and reused for each test. The wall panel connections were screwed to the panel using 18 Strong-Drive® SDS Structural Wood Screws per side. The floor connections were welded to the steel of the strong floor. Four 25.4 mm diameter A36 steel pins were used with the loading apparatus to transfer load at the top of the panel. Energy dissipators were attached to both faces of the CLT panel, referred to as the North and South sides. The panel test setup can be seen in Fig. 3.3.

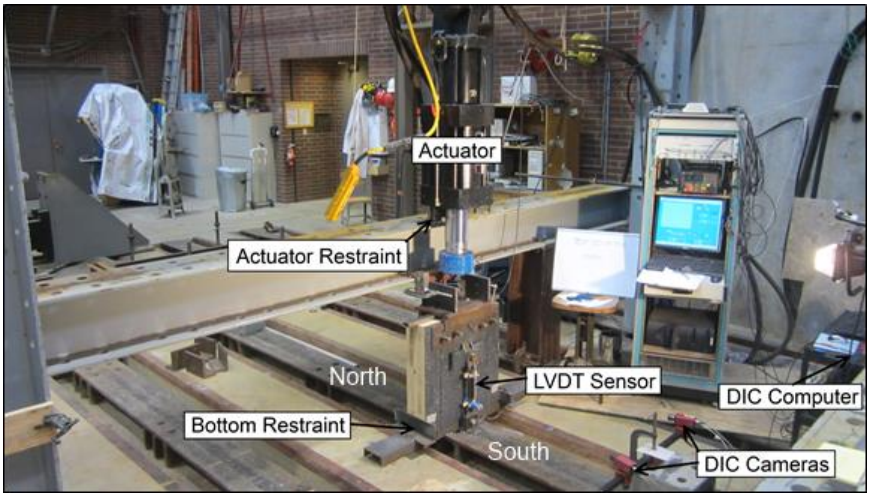

Fig. 3.3. Panel test setup

3.5 Methods

3.5.1 Individual Tension Tests

Three tension tests were performed to verify the yield and strength characteristics of steel coupons, and obtain force-deflection data for system comparison. Localized strain behavior was also observed. The parameters for testing were selected according to ASTM A370-12a (ASTM 2012). The speed of testing was 0.076 mm/sec until 2.54 mm Universal Testing Machine (UTM) displacement to ensure capture of the yield point and 0.254 mm/sec afterwards until failure. A 50 mm gauge length extensometer was used to

obtain yield properties, and calipers were used to measure the final elongation. The tests were performed using an Instron 5582 UTM and flat serrated wedge type grips.

3.5.2 Panel Tension Tests

Three panel tension tests were conducted and followed ASTM A370-12a procedures with one energy dissipator connected to each face of the CLT panel. The speed of testing was modified due to a lower combined stiffness of the system from the connection and panel properties, which resulted in a longer time to reach the yield point. The speed of testing was 0.015 mm/sec until yield and then 0.13 mm/sec until failure. Energy dissipators were attached to both faces of the panel, to discourage eccentricity during testing. The tests were performed using a MTS displacement-controlled 490 kN capacity actuator attached to the apparatus seen in Fig. 1, which applied vertical displacements while longitudinal and transverse (out-of-plane) actuator movement near the top of the panel was physically restrained. Restraints were also used at the bottom of the panel to minimize side sway, but a 3 mm gap was allowed on either side. The panels were brought to a minimal tension load before initiating the test, measured using a load cell in the actuator.

3.5.3 Panel Cyclic Tests

Five cyclic tests were conducted according to the modified ACI T1.1-01 cycle sequence (ACI 2001). The panel cyclic tests were configured with an energy dissipator attached to each face of the CLT panel as seen in Fig. 3.3. LVDT sensors with ±25.4 mm stroke were used to track the elongation of both energy dissipator milled sections, since an extensometer could not be used due to the presence of the grouted sleeve. Cyclic testing of self-centering systems has been performed previously using ACI T1.1-01 (Smith et al. 2007). Due to the geometry of the designed system, a modified version of ACI T1.1-01 was developed to emulate the motion at the location of the energy dissipators. The modified full test sequence for 15 cycles and the individual cycle sequence (normalized) are shown in Fig. 3.4.

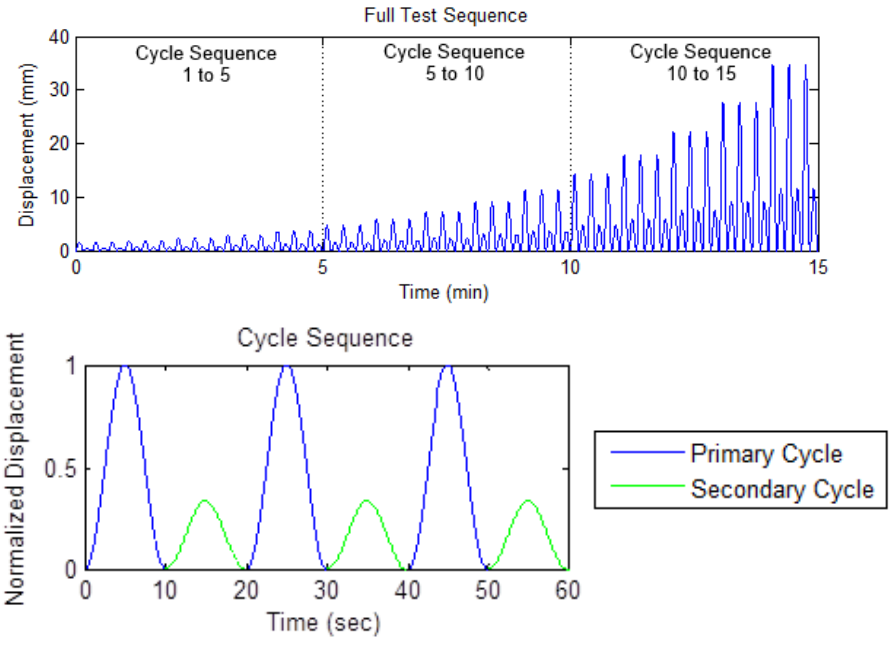

Fig. 3.4. Modified T1.1-01 full test sequence (a) and individual cycle sequence (b)

The cycles began at 1.9 mm and each subsequent cycle sequence was increased by 25% until reaching failure. Testing was paused briefly between each cycle sequence to document damage progression. The tests were performed using the same setup as the panel tension tests. A schematic of the test setup is presented in Fig. 3.5.

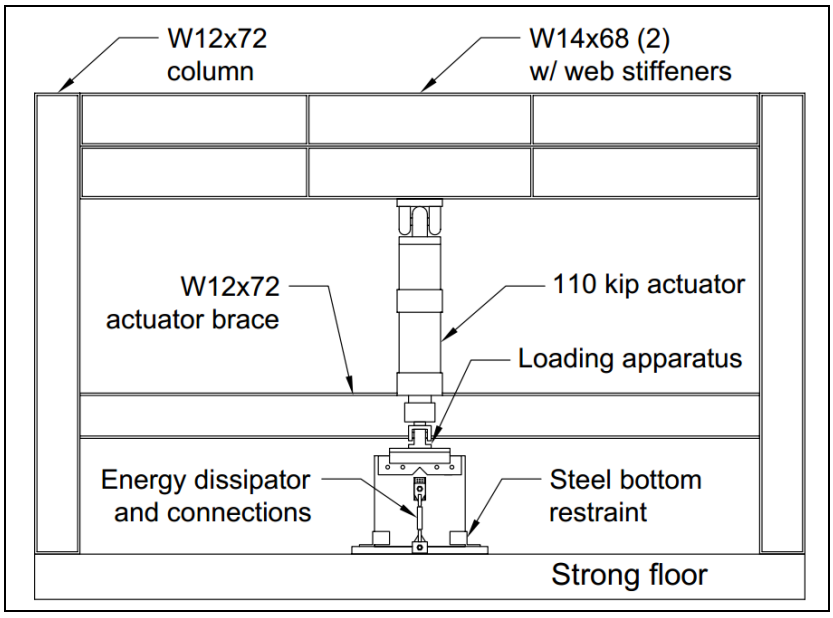

Fig. 3.5. Test setup and configuration (elevation view)

3.5.4 Digital Image Correlation

All panel tests were monitored using Digital Image Correlation (DIC) techniques, which have been successfully applied to analyze strain and displacement in wood-frame construction (Sinha and Gupta 2009). In panel tension tests, DIC was used to capture the elongation of the energy dissipator milled section and the local strain behavior. DIC was additionally used in panel cyclic tests to track the displacement of the panel, due to small rotation and out of plane movement observed. This procedure was conducted on only the south energy dissipator.

3.6 Results and Discussion

3.6.1 Individual Tension Tests

The tension tests were conducted on individual energy dissipators to obtain force, displacement, and strain data. Understanding force-displacement relationships are critical for incorporation within a post-tensioned system (Sarti et al. 2013). Stress-strain relationships were also calculated based on extensometer data. The results of the force-displacement curves are presented in Fig. 3.6.

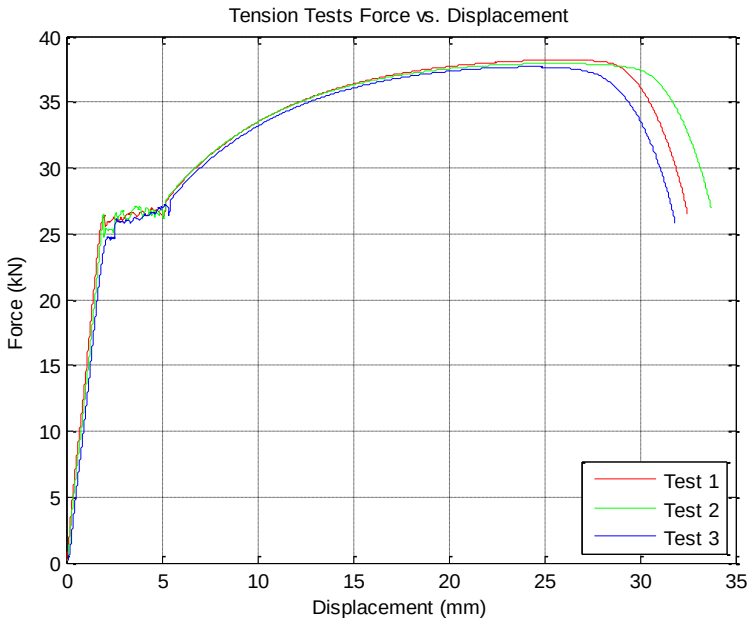

Fig. 3.6. Force-displacement curves for individual tension tests

Fig. 3.6 shows the full specimen displacement. The extensometer data approximated the Young's Modulus to be 205 MPa. The mean values for yield strength obtained using the 0.2% offset method, ultimate strength, and fracture strength were 370 MPa, 530 MPa, and 370 MPa respectively. The strain at failure was measured using calipers over a 150 mm gauge length and the mean was 20%, which is expected for A36 (ASTM 2012), with a Coefficient of Variation (COV) of 3.8% which is typical for steel (Schmidt and Bartlett 2002). This procedure was useful in understanding full panel behavior in subsequent sections.

3.6.2 Panel Tension Tests

The panel tension tests were conducted on energy dissipators attached to panels to observe the effect of the connection system on the yielding and failure behavior of the energy dissipators. The force-displacement curves are presented in Fig. 3.7.

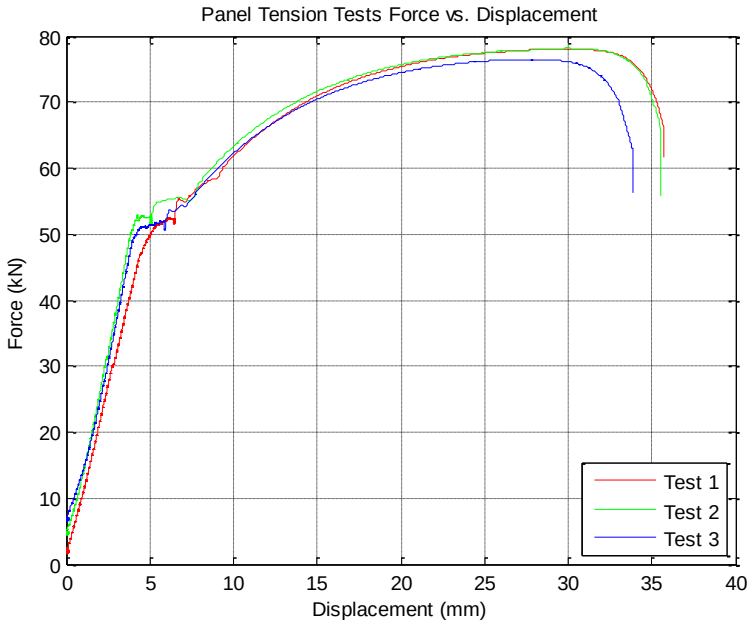

Fig. 3.7. Force-displacement curves for panel tension tests

The force-displacement curves (Fig. 3.7) were adjusted for initial alignment, which is shown by the difference in plotted initial force. This was done to improve the clarity of variation in the force-displacement behavior. Initial slack is caused by one energy dissipator engaging before the other, due to tolerances in manufacturing and installation. This also influenced the failure results, due to the fact that one dissipator, attached on either side of the panel, always failed several seconds before the other, which is mainly due to slight eccentricities and tolerances described previously. The mean engineering values for yield strength, ultimate strength, and fracture strength were 365 MPa, 545 MPa, and 460 MPa, respectively. The fracture strength in the panel tension tests is higher than the individual tests due to failure of one energy dissipator before the other in the panel tests. These values were approximated with the assumption that force was divided equally between energy dissipators. The deflection at failure was higher than for individual tests, which is expected due to the combined deformations from the panel and connection system. The failure strains measured using calipers gave a mean value of 21% with a COV of 6.0%. The COV was higher in the panel tests due to the fact that the first energy dissipator to fail always had a lower strain at failure. Eccentricity due to

fabrication and slight rotation of the panel during testing also may have contributed to the small differences in failure behavior.

DIC techniques were used on the panel tension tests to track the strain progression of the energy dissipators. This technique was considered after notable observation of strain localization and necking near the shoulder of the milled section at failure. The results are presented in Fig. 3.8.

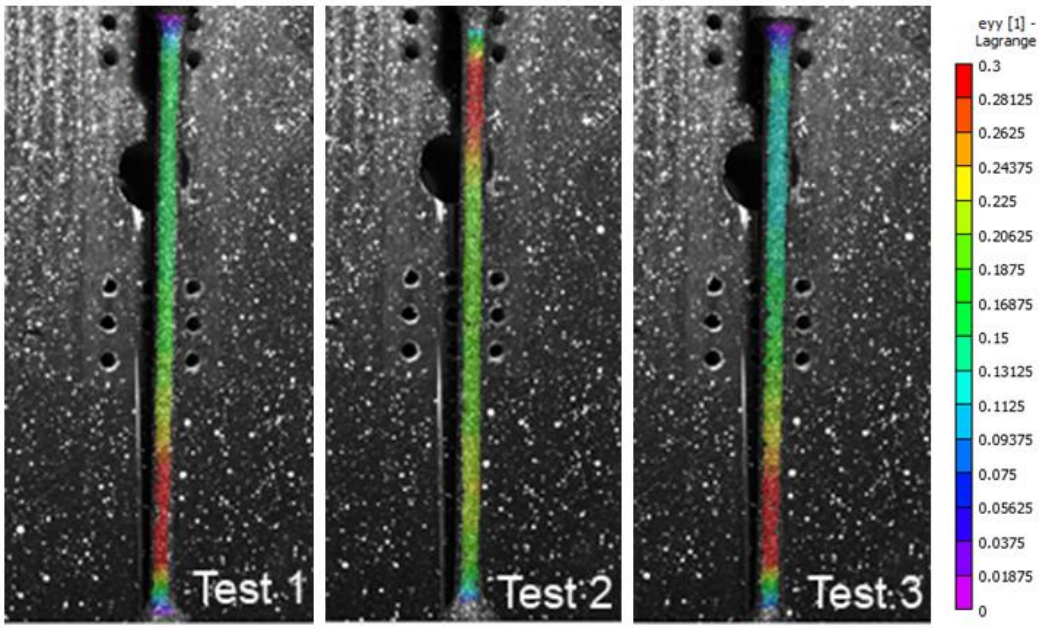

Fig. 3.8. DIC strain near failure for panel tension tests 1-3

Although there is a large amount of strain localization near the point of failure, there is still a moderate amount of strain throughout the full 150 mm milled length. This is the reason for a 20% elongation at failure when considering the full milled length.

3.6.3 Panel Cyclic Tests

Results from the cyclic panel tests can be found in Table 3.1.

Table 3.1. Summary of panel cyclic test results

Test	Side	ΔL (mm)	Eng. Strain (ε)	Energy Dissipated (J)	Force at Ultimate (kN)
1	*N	24.36	16.0%	4100	74.1
	S	25.22	16.6%		
2	N	26.67	17.5%	3703	75.1
	*S	24.38	16.0%		
3	N	24.13	15.8%	3394	73.2
	*S	24.13	15.8%		
4	N	24.13	15.8%	3472	73.5
	*S	23.80	15.6%		
5	N	29.72	19.5%	3975	76.7
	*S	24.82	16.3%		
Standard Deviation		1.81	1.19%	307.0	1.42
Average		25.14	16.5%	3729	74.5
Coefficient of Variation		7.20%	7.20%	8.23%	1.90%

*indicates first failure

The failure results in Table 3.1 show the engineering strain at failure which was measured using calipers. First failure is an indication of whether the north or south energy dissipator failed first. Both failures typically occurred in cycle sequence 15, and within a few seconds of each other. The side that failed first always had a lower elongation at failure. This was probably due to slight rotation of the panel from one energy dissipator engaging before the other as a result of slightly different tolerances and eccentricity of the connection system. Typical cyclic test behavior can be seen in Fig. 3.9, which represents Test 3 and separates the cycle sequences from 1 to 15.

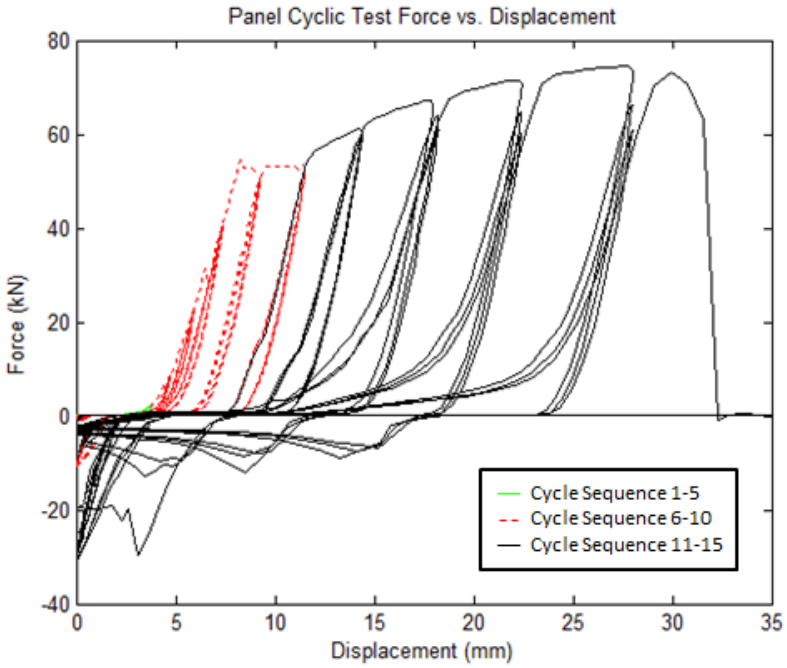

Fig. 3.9. Force-displacement curves (Test 3)

The larger amplitude displacements (primary cycles) are clearly seen in Fig. 3.9, and the first primary cycle dissipates the majority of the energy in the cycle sequence. Smaller amplitude displacements (secondary cycles) are not seen, due to secondary cycles not overcoming the slack of the system.

3.6.3.1 Connection Slack

Tolerances of the connection system were measured, and a total potential slack of 11.5 mm was determined. Approximately 2.7 mm of the total potential slack is an artifact of the testing apparatus. The initial slack of the system is due to tolerances at the time of installation. Most tests had approximately 3.2 mm initial slack, which can be attributed to the upper and lower hole tolerances of 1.6 mm common for steel fabrication. As the test progresses, the slack grows along with the plastic deformation of the energy dissipators. At any point in the test, the cumulative slack can be observed by the length of the section along the x-axis during unloading, when the force changes from tension to compression. An additional source of slack is the wall connection, which can be subjected to small

localized displacements. This is due to the localized stress surrounding the structural fasteners and the all-thread bolt through the center of the panel. Targets were welded to the sides of the south connection and monitored optically. The displacement of the targets was compared with the actuator displacement, and up to 2.54 mm of relative displacement was observed. This may also have been due to deformation of the CLT panel, or the pins which hold the loading apparatus in place.

3.6.3.2 Buckling Behavior

All tests exhibited buckling behavior, typically in the form of lateral buckling. This occurred near the shoulder of the milled section, where strain localization was observed (Fig 3.10).

Fig. 3.10. Buckling behavior (Test 3)

The primary cause for the buckling behavior was the permanent tensile deformation of the milled section, which exposed an unbraced portion of the energy dissipator and also allowed for compression loads after overcoming slack in the system. The buckling was also enabled by the pinned connections which allowed rotation. Additionally, it may have been influenced by eccentricity of the energy dissipators which were a result of fabrication. Buckling consistently occurred during cycle sequence 11, which was at the

initiation of strain hardening in the energy dissipator. This provides insight to the onset of buckling, due to strong dependence on the maximum tensile strain reached before reversal. This observation was also supported by Rodriguez et al. (1999). The effect seen on the force-displacement curve in Fig. 3.9 is a lower initial stiffness during loading, representative of the axial force required to pull the milled section straight. Additionally, the compressive strength decreases throughout the cycle sequences, as indicated by the peaks on the compressive side, which represents the onset of buckling. The reduction in compressive strength is due to greater elongation in the milled section, which allows for buckling at a lower compressive load.

3.6.3.3 Energy Dissipation

Approximations were made for energy dissipation of the primary cycles using trapezoidal numerical integration in Matlab and are presented in Fig. 3.11 segregated according to each primary loop number. This is according to Fig. 3.4. where there are three primary loops per cycle sequence.

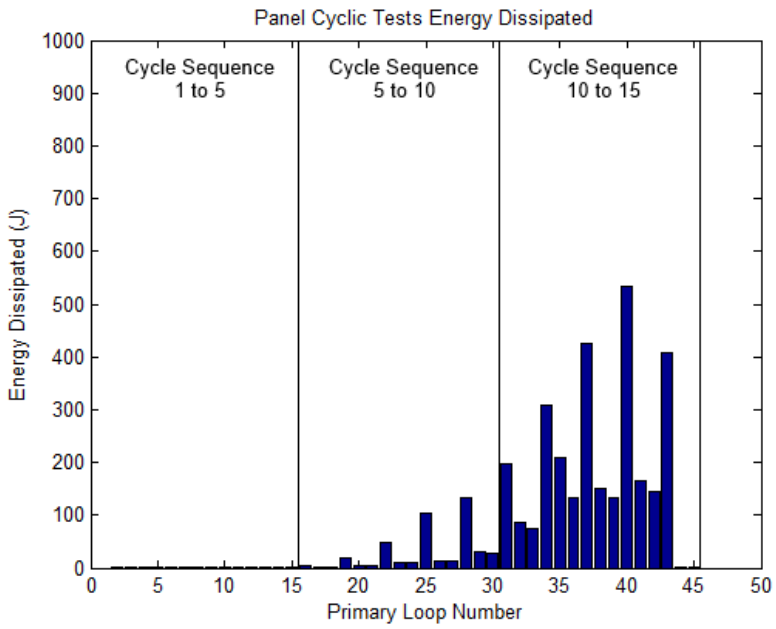

Fig. 3.11. Energy dissipated per loop (Test 3)

The initial cycles show the elastic range of the energy dissipator where almost no energy is dissipated. Yield occurs during cycle sequence 9 (loop numbers 25-27). Buckling occurs during cycle sequence 11 (loop numbers 31-33). The effects of buckling are apparent in the second and third primary cycles, where the energy dissipated no longer increases (cycle sequences 12-14). Values for calculated total energy dissipation can be found in Table 3.1. The variation in energy dissipation is likely due to the effects of buckling and the minor eccentricity in the system. Average total energy dissipated for tests was 3730 Joules.

3.6.4 Revised Panel Cyclic Test

In order to better understand the buckling behavior and its effect on the system, an additional prototype was fabricated and tested. The revised design had a smaller and longer sleeve which was a 19 mm diameter schedule 40 thickness pipe and covered the virgin section of the shoulder by approximately 50 mm. An image of the revised design is shown in Fig. 3.12.

Fig. 3.12. Revised energy dissipator design

3.6.4.1 Buckling Behavior

The revised design showed reduced buckling, and did not demonstrate any buckling behavior until later in the test. The observed buckling was restricted due to the sleeve, but caused deformation in the ends of the sleeve. Failure still occurred in cycle sequence 15 at approximately the average load and deflection of previous specimens. The maximum compressive forces were approximately double those from previous tests, and buckling effects are less frequent as shown in the force-displacement curves in Fig. 3.13.

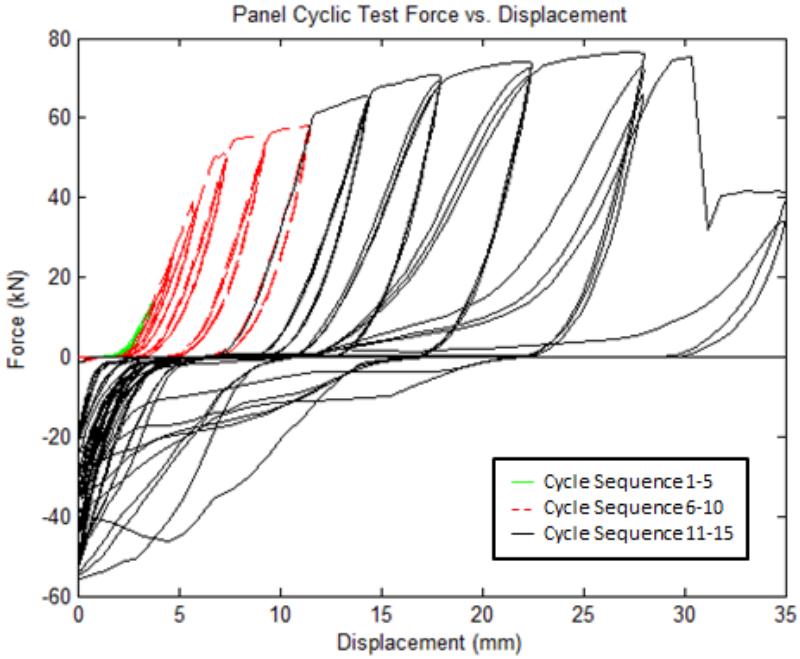

Fig. 3.13. Force-displacement curves (revised design)

3.6.4.2 Energy Dissipation

The revised design performed much better in terms of energy dissipation. The calculated energy dissipation was 6250 Joules, which is about a 70% increase compared to the mean obtained in the previous test results. Energy dissipation for each primary loop can be found in Fig. 3.14.

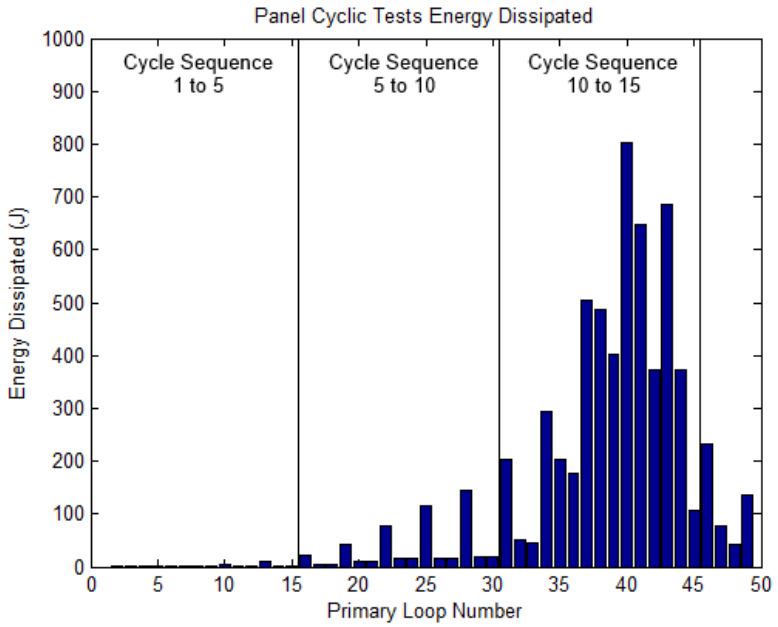

Fig. 3.14. Energy dissipated per loop (revised design)

An important aspect of these tests is to control and understand the displacement and deformation behavior of the energy dissipator and connection system. A common difficulty when designing steel to wood connections is ensuring rigidity and avoiding damage or failure around the fasteners. No damage was observed on the CLT panel during testing, and the fasteners remained rigidly attached after each test sequence. The slack observed in the tests inhibits the energy dissipation, due to the changing reloading condition and the delay when changing from tension to compression.

The effect of buckling on the energy dissipation of the system is the greatest cause for concern. Prevention and accurate prediction of buckling will ensure the greatest energy dissipation possible in these types of energy dissipators while ensuring that the behavior of these components is predictable.

3.7 Conclusion

Overall the energy dissipators performed adequately and the connection system showed little sign of fatigue from repeated use, confirming this design as adequate for potential application in rocking wall systems. The individual tension tests produced predictable results with low variability. Panel tension tests gave insight to the local strain behavior in milled sections through DIC tracking, which is an important factor in energy dissipator design considerations. The results from the panel cyclic tests showed relatively low variability in ultimate force and elongation of the energy dissipators. Slack in the system affected the energy dissipation and produced discontinuity in force resistance, but can be accounted for with consideration of bolt hole tolerances.

Buckling should be controlled to ensure predictable performance. This can be done through increasing the size of the sleeve, which increases energy dissipation as shown by the revised design. A thicker sleeve may also be necessary due to deformations at the ends of the sleeve. The CLT panel was not visibly damaged during testing, and is a proper material to be used for this type of connection system. It may be possible to increase the size of energy dissipator but the connections would likely have to be redesigned, due to small displacements of the wall connection tracked by the DIC system.

3.8 Future Work

These panel tests presented a restricted lateral and out-of-plane movement to capture the cyclic vertical displacement behavior of the energy dissipators. Future work should be done to observe the behavior of out-of-plane movement of energy dissipators connected to the face of wall panels. The performance may change slightly due to out-of-plane movement causing compressive strains in the energy dissipator, and the flanges may be susceptible to buckling. Future work should also be done on full wall panels to ensure the rocking capability of the system.

3.9 References

American Concrete Institute (ACI), Innovation Task Group 1. (2001). "Acceptance criteria for moment frames based on structural testing (ACI T1.1-01) and Commentary (ACI T1.1R-01)." Farmington Hills, MI.

ASTM International. (2012). "Standard Test Methods and Definitions for Mechanical Testing of Steel Products." *A370-12a.* West Conshohocken, PA.

ASTM International. (2012). "Specification for Carbon Structural Steel. ASTM International." *ASTM A36/A36M-12.* West Conshohocken, PA

Ceccotti, A., Sandhaas, C., Okabe, M., Yasumura, M., Minowa, C., and Kawai, N. (2013). "SOFIE project - 3D shaking table test on a seven-storey full-scale cross-laminated timber building: 3D SHAKING TABLE TEST ON A SEVEN-STOREY FULL-SCALE X-LAM BUILDING." *Earthquake Engineering & Structural Dynamics,* 42(13), 2003–2021.

Devereux, C. P., Holden, T. J., Buchanan, A. H., and Pampanin, S. (2011). "NMIT Arts & Media Building-Damage Mitigation Using Post-tensioned Timber Walls." *9th Pacific Conference on Earthquake Engineering,* Auckland, New Zealand.

Guerrini, G., Restrepo, J. I., Massari, M., and Vervelidis, A. (2012). "Self-Centering Precast Concrete Dual-Shell Steel." *15th World Conference on Earthquake Engineering,* Lisbon, Portugal.

Holden, T., Restrepo, J., and Mander, J. B. (2003). "Seismic Performance of Precast Reinforced and Prestressed Concrete Walls." Journal of Structural Engineering, 129(3), 286–296.

Kramer, A., Barbosa, A. R., and Sinha, A. (2013). "Viability of Hybrid Poplar in ANSI Approved Cross-Laminated Timber Applications." *Journal of Materials in Civil Engineering,* in press.

Kurama, Y., Pessiki, S., Sause, R., & Lu, L. W. (1999). "Seismic behavior and design of unbonded post-tensioned precast concrete walls." *PCI journal,* 44(3), 72-89.

Kurama, Y. C. (2000). "Seismic design of unbonded post-tensioned precast concrete walls with supplemental viscous damping." *ACI Structural Journal*, 97(4).

Marriott, D., Pampanin, S., Bull, D., and Palermo, A. (2008). "Dynamic testing of precast, post-tensioned rocking wall systems with alternative dissipating solutions." *New Zealand National Conference of Earthquake Engineering.* Wellington, New Zealand.

Marriott, D., Pampanin, S., and Palermo, A. (2009). "Quasi-static and pseudo-dynamic testing of unbonded post-tensioned rocking bridge piers with external replaceable dissipaters." *Earthquake Engineering & Structural Dynamics,* 38(3), 331–354.

Palermo, A., Pampanin, S., and Marriott, D. (2007). "Design, modeling, and experimental response of seismic resistant bridge piers with posttensioned dissipating connections." *Journal of Structural Engineering,* 133(11), 1648–1661.

Palermo, A., Sarti, F., Baird, A., Bonardi, D., Dekker, D., and Chung, S. (2012). "From theory to practice: design, analysis and construction of dissipative timber rocking post-Tensioning wall system for Carterton Events Centre, New Zealand." 15th *World Conference on Earthquake Engineering.* Lisbon, Portugal.

Rahman, A. and Restrepo, J. I. (2000). ''Earthquake resistant precast concrete buildings: Seismic performance of cantilever walls pre-stressed using unbonded tendons.'' *Research Rep. No. 2000-5,* Dept. of Civil Engineering, Univ. of Canterbury, Christchurch, New Zealand.

Restrepo, J. I., and Rahman, A. (2007). "Seismic performance of self-centering structural walls incorporating energy dissipators." *Journal of Structural Engineering,* 133(11), 1560–1570.

Rodriguez, M. E., Botero, J. C., and Villa, J. (1999). "Cyclic Stress-Strain Behavior of Reinforcing Steel Including Effect of Buckling." *Journal of Structural Engineering,* 125(6), 605–612.

Sarti, F., Smith, T., Palermo, A., Pampanin, S., and Carradine, D. M. (2013). "Experimental and analytical study of replaceable Buckling-Restrained Fuse-type (BRF) mild steel dissipaters." *New Zealand Society for Earthquake Engineering Technical Conference,* Wellington, New Zealand.

Schmidt, B. J., and Bartlett, F. M. (2002). "Review of resistance factor for steel: data collection." *Canadian Journal of Civil Engineering,* 29(1), 98–108.

Sinha, A., and Gupta, R. (2009). "Strain distribution in OSB and GWB in wood-frame shear walls." *Journal of Structural Engineering,* 135(6), 666–675.

Smith, T., Ludwig, F., Pampanin, S., Fragiacomo, M., Buchanan, A., Deam, B., and Palermo, A. (2007). "Seismic response of hybrid-LVL coupled walls under quasi-static and pseudo-dynamic testing." *New Zealand Society for Earthquake Engineering Conference,* Palmerston North, New Zealand.

4 General Conclusion

The purpose of this study was to investigate potential improvements to cross-laminated limber (CLT) through new materials and technology. This was achieved by developing two different studies, the first investigating the use of low-density hardwood species for use in CLT panels, and the second developing a testing a novel energy dissipator for use in hybrid self-centering CLT walls. The conclusions of the study in alignment with the specific objectives are as follows:

1. In Chapter 2, an investigation into low density species as feedstock showed promising results. The results from structural testing of hybrid poplar CLT panels show that low-density CLT will potentially meet and exceed the shear and bending strength requirements for ANSI/APA PRG-320 Grade E3. Block shear tests showed adequate bond strength using a structural grade adhesive. Stiffness requirements were not met, however, which is related to the density of the material.

2. Further investigation into CLT panels with multi wood species layers could potentially produce lighter weight panels and a higher structural efficiency. It is important to consider the location of boards during layup to control failure modes. Future testing campaigns should include a large number of tests to verify the impacts of board layup on full panel strength. One issue that may arise with low-density (hence low modulus of elasticity) panels is serviceability requirements where deflection is a primary concern. Overall, the hybrid poplar CLT panels performed adequately, and have potential for use based on initial strength values obtained through these tests.

3. In Chapter 3, another technology that was investigated was hybrid self-centering solutions for use in CLT walls. This technology has potential for use in CLT due to high shear stiffness, which is important to rocking behavior. A hybrid system was design based on similar procedures used for precast concrete hybrid systems.

   The connections designed for attachment to the wall and floor were novel pin based connections, which allowed the energy dissipators to rotate and alleviated an induced moment seen in fixed connection design. However, the fabrication of the connections included hole tolerance based on the energy dissipator attachment, leading to inherent slack in the connection system. The energy dissipators designed for the system performed adequately on a strength basis, but the energy dissipated by the system was inhibited due to slack which built up. The wall and floor connections performed well during repeated use, and showed no signs of fatigue or failure, confirming potential application.

4. Results from the energy dissipator tests show little variability in yield and ultimate stress and strain, ensuring predictability of the system for use in design. Digital Image Correlation techniques used on the tension tests captured local strain behavior in the milled section near the shoulder. These data are useful in estimating future strain behavior in similar energy dissipative devices, to aid in estimating elongation of the energy dissipators at failure.

   Buckling effects of the energy dissipator were observed and shown to be predictable. This observation led to a revision in the first design, with better controlled buckling behavior, resulting in a 70% increase in energy dissipation.

   Future work should take into consideration both the effects of buckling and slack on the energy dissipation of the system to ensure a high performance device. These devices should also be tested with full panel systems to ensure rocking capability.

In summary, cross-laminated timber is a relatively new engineered wood product, particularly in North America, and there are many opportunities to develop alternative design solutions to improve its structural properties and viability. Herein, two alternatives were tested, but other developments are needed to make CLT solutions a reality in industry applications. Furthermore, as CLT is now entering the marketplace in the US, innovations in design will allow CLT structures to be resilient to earthquakes and provide new and sustainable building solutions.

5 Bibliography

American National Standards Institute (ANSI). (2008). "Standard for adhesives for use in structural glued laminated timber." ANSI 405-2008. New York, NY.

ASTM International. (2012). "Standard test methods for mechanical properties of lumber and wood-base structural material." *ASTM D4761-05,* West Conshohoken, PA.

APA -The Engineered Wood Association. (2012), "Standard for Performance-Rated Cross-Laminated Timber." ANSI/APA PRG 320. Tacoma, WA.

Ceccotti, A. (2008). "New Technologies for Construction of Medium-Rise Buildings in Seismic Regions: The XLAM Case." *Structural Engineering International,* 18(2), 156–165.

Ceccotti, A., Lauriola, M. P., Pinna, M., and Sandhaas, C. (2006). "SOFIE Project–Cyclic Tests on Cross-Laminated Wooden Panels." *9th World Conference on Timber Engineering,* Portland, OR.

Ceccotti, A., Sandhaas, C., Okabe, M., Yasumura, M., Minowa, C., and Kawai, N. (2013). "SOFIE project - 3D shaking table test on a seven-storey full-scale cross-laminated timber building". *Earthquake Engineering & Structural Dynamics,* 42(13), 2003–2021.

Devereux, C. P., Holden, T. J., Buchanan, A. H., and Pampanin, S. (2011). "NMIT Arts & Media Building-Damage Mitigation Using Post-tensioned Timber Walls." 9th Pacific Conference on Earthquake Engineering, Auckland, New Zealand.

Dujic, B., Strus, K., Zarnic, R., and Ceccotti, A. (2010). "Prediction of Dynamic Response of a 7-Storey Massive XLam Wooden Building Tested on a Shaking Table." *World Conference on Timber Engineering,* Riva del Gara, Trentino, Italy.

Fragiacomo, M., Dujic, B., and Sustersic, I. (2011). "Elastic and ductile design of multi-storey crosslam massive wooden buildings under seismic actions." *Engineering Structures,* 33(11), 3043–3053.

Fragiacomo, M., Smith, T., Buchanan, A. H., and Pampanin, S. (2009). "Construction time and cost for post-tensioned timber buildings." *Proceedings of the ICE - Construction Materials,* 162(4), 141–149.

Gagnon, S. and Pirvu, C., Eds. (2011). "CLT Handbook: Cross-Laminated Timber." *FPInnovations,* Vancouver, BC.

Gavric, I., Ceccotti, A., and Fragiacomo, M. (2011). “Experimental cyclic tests on cross-laminated timber panels and typical connections.” *Proceedings of the 14th L’Ingegneria Sismica in Italia (ANIDIS) Conference,* Bari, Italy.

Green, M., and J. E. Karsh. (2012) "The case for tall wood buildings." *mgb Architecture + Design.* Vancouver, BC, Canada.

Harris, M. (2012). "Wood goes high-rise." *Engineering & Technology,* 7(9), 43-45

Iqbal, A., Pampanin, S., Palermo, A., and Buchanan, A. H. (2010). “Seismic Performance of Full-scale Posttensioned Timber Beam-column Joints.” *11th World Conference on Timber Engineering,* Riva del Garda, Trentino, Italy.

Kreuzinger, H. (1999) "Platten, Scheiben und Schalen: Ein Berechnungsmodell für gängige Statikprogramme." *Bauen mit Holz.* 1. 34-39.

Langenbach, R. (2008). “Resisting Earth’s Forces: Typologies of Timber Buildings in History.” *Structural Engineering International,* 18(2), 137–140.

Lauriola, M. P., & Sandhaas, C. (2006). “Quasi-static and pseudo-dynamic tests on XLAM walls and buildings.” *In COST E29 International Workshop on Earthquake Engineering on Timber Structures,* Coimbra, Portugal.

Nakaki, S. D., Stanton, J. F., & Sritharan, S. (1999). “An overview of the PRESSS five-story precast test building.” *PCI journal,* 44(2), 26-39.

Newcombe, M. P., Pampanin, S., and Buchanan, A. H. (2010). “Global Response of a Two Storey Pres-Lam Timber Building.” *New Zealand Society for Earthquake Engineering Conference,* Wellington, New Zealand.

Palermo, A., Pampanin, S., Fragiacomo, M., Buchanan, A. H., and Deam, B. L. (2006). “Innovative seismic solutions for multi-storey LVL timber buildings.” *World Conference on Timber Engineering,* Portland, OR.

Palermo, A., Sarti, F., Baird, A., Bonardi, D., Dekker, D., and Chung, S. (2012). “From theory to practice: design, analysis and construction of dissipative timber rocking post-Tensioning wall system for Carterton Events Centre, New Zealand.” *World Conference on Earthquake Engineering,* Lisbon, Portugal.

Pei, S., Popovski, M., and van de Lindt, J. W. (2012). “Seismic design of a multi-story cross laminated timber building based on component level testing.” *World Conference on Timber Engineering.* Auckland, New Zealand.

Rinaldin, G., Amadio, C., & Fragiacomo, M. (2013). "A component approach for the hysteretic behaviour of connections in cross-laminated wooden structures." *Earthquake Engineering & Structural Dynamics*, 42(13), 2023-2042.

Schneider, J., Stiemer, S. F., Tesfamariam, S., Karacabeyli, E., and Popovski, M. (2012). "Damage Assessment of Cross Laminated Timber Connections Subjected to Simulated Earthquake Loads". *World Conference on Timber Engineering.* Auckland, New Zealand.

Smith, T., Ludwig, F., Pampanin, S., Fragiacomo, M., Buchanan, A., Deam, B., and Palermo, A. (2007). "Seismic response of hybrid-LVL coupled walls under quasi-static and pseudo-dynamic testing." *New Zealand Society for Earthquake Engineering Conference,* Palmerston North, New Zealand.

Smith, T., Pampanin, S., Fragiacomo, M., and Buchanan, A. (2008). "Design and construction of prestressed timber buildings for seismic areas." *University of Canterbury.* Christchurch, New Zealand.

Steiger, R., and Gülzow, A. (2009). "Validity of bending tests on strip-shaped specimens to derive bending strength and stiffness properties of cross-laminated solid timber (X-lam)." *Proceedings of CIBW18 Timber Engineering,* University of Karlsruhe, Karlsruhe, Germany. 42–12.

Yates, M., Linegar, M., and Dujic, B. (2008). "Design of an 8 storey residential tower from KLH — Cross laminated solid timber panels." *World Conference on Timber Engineering*, Miyazaki, Japan.

Yeh, B., Gagnon, S., Williamson, T., and Pirvu, C. (2012). "The North American Product Standard for Cross-Laminated Timber". *Wood Design Focus,* 22(2), 13-21.

APPENDICES

6 Appendices

6.1 Additional Figures Chapter 2

6.1.1 Third Point Bending Figures

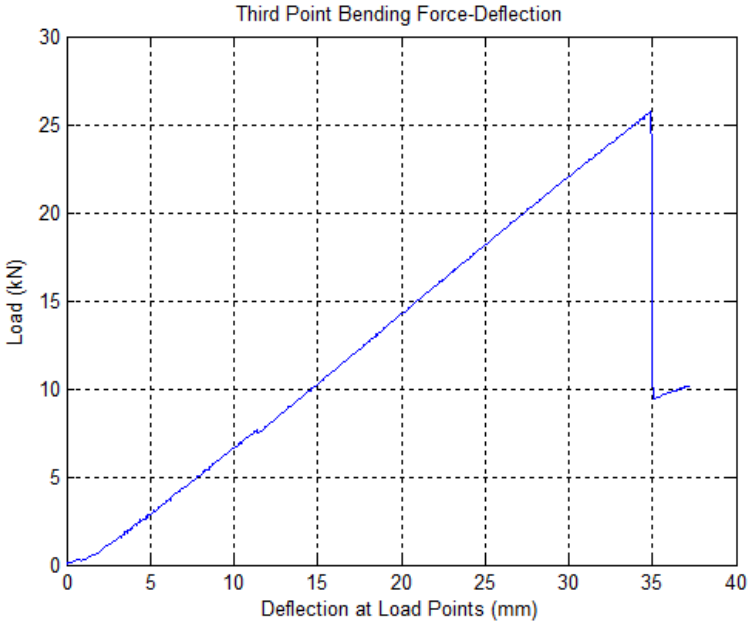

Fig. 6.1. Third point bending test force-deflection (Test 1)

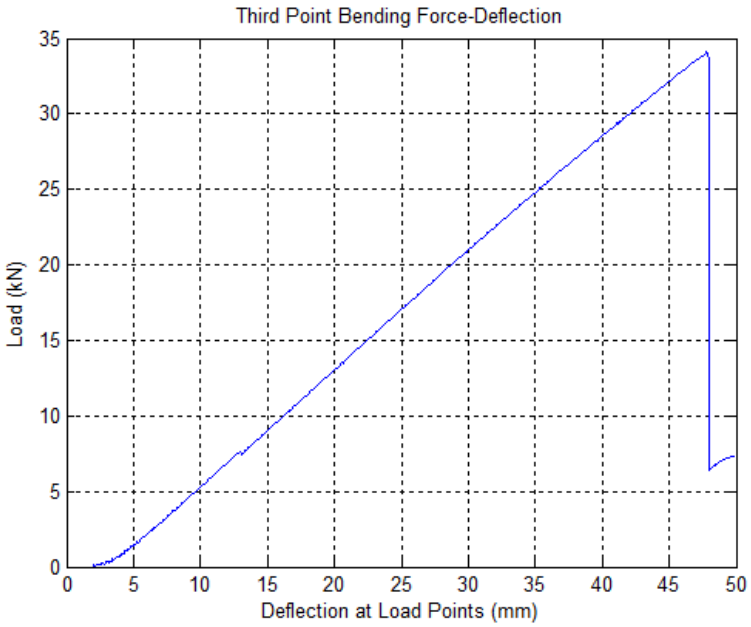

Fig. 6.2. Third point bending test force-deflection (Test 2)

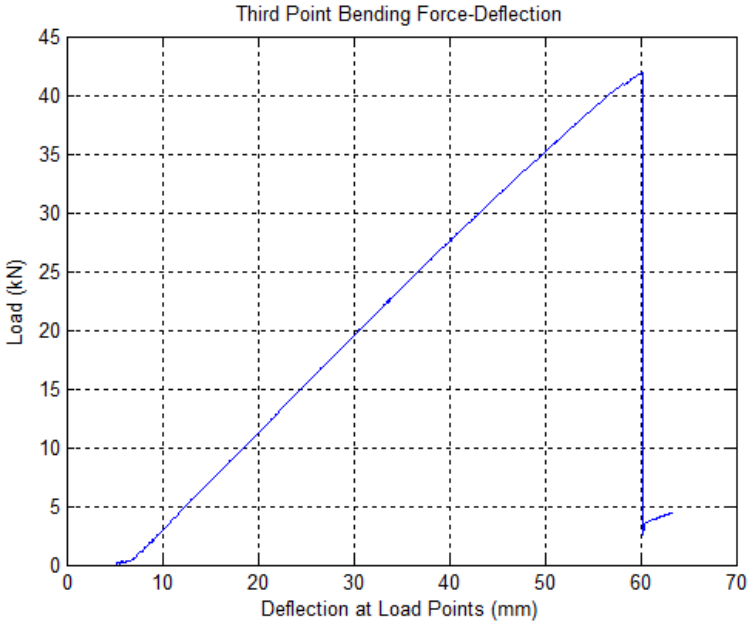

Fig. 6.3. Third point bending test force-deflection (Test 3)

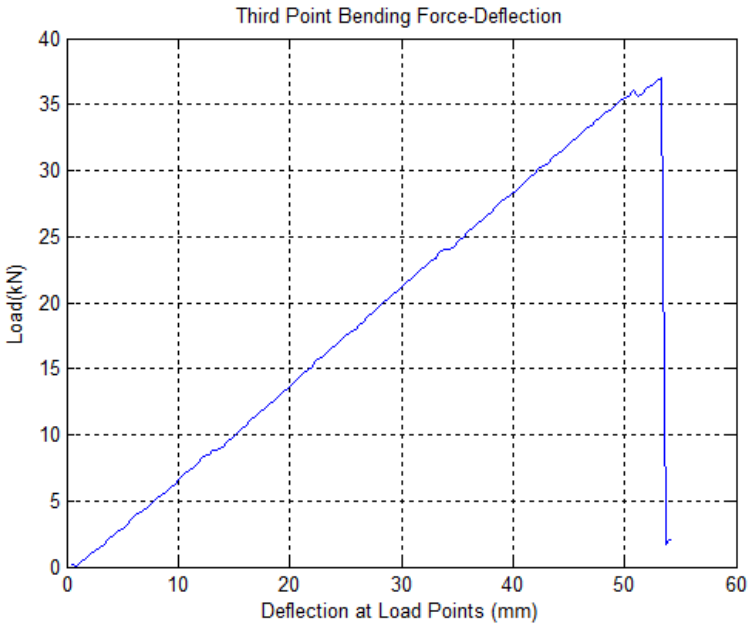

Fig. 6.4. Third point bending test force-deflection (Test 6)

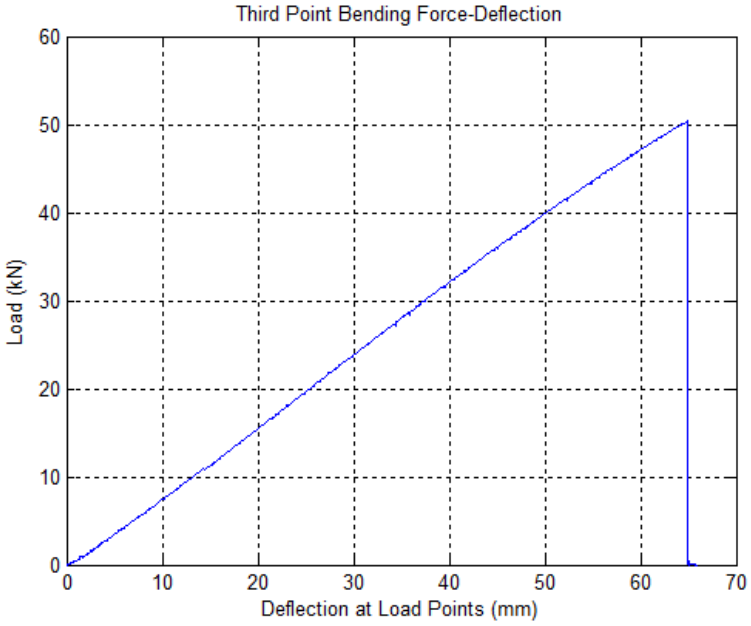

Fig. 6.5. Third point bending test force-deflection (Test 7)

6.1.2 Short Span Bending Figures

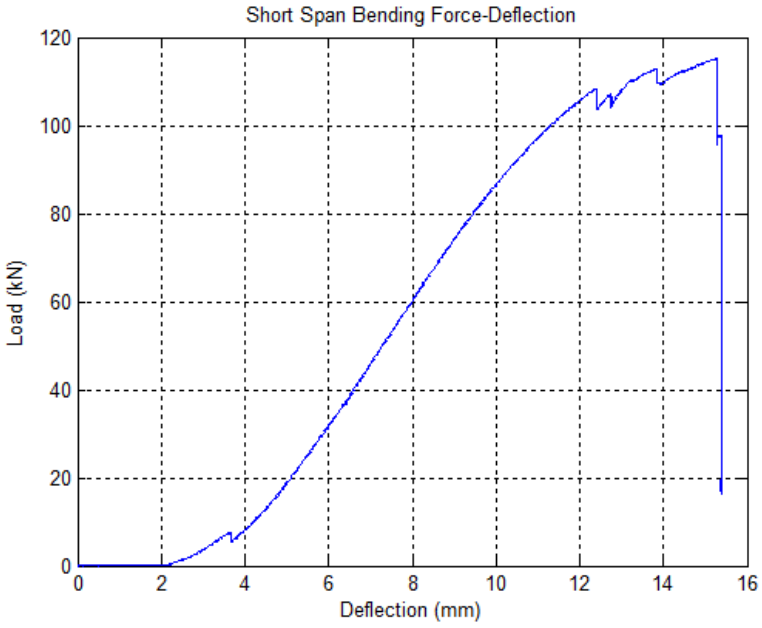

Fig. 6.6. Short span bending test force-deflection (Test 4-1)

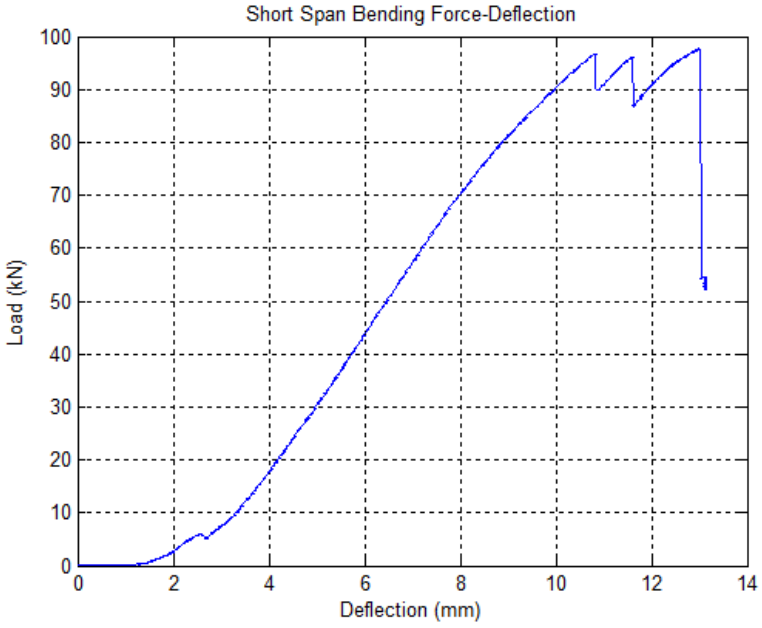

Fig. 6.7. Short span bending test force-deflection (Test 4-2)

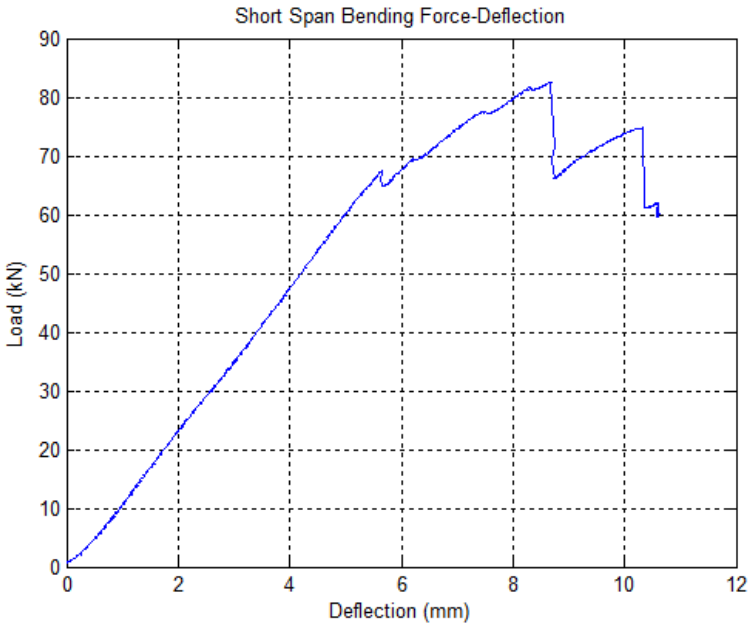

Fig. 6.8. Short span bending test force-deflection (Test 4-3)

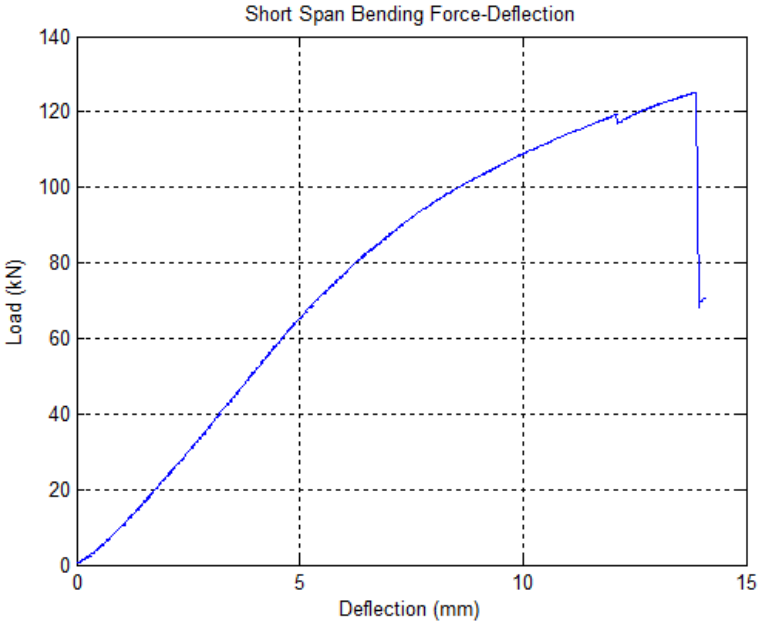

Fig. 6.9. Short span bending test force-deflection (Test 4-4)

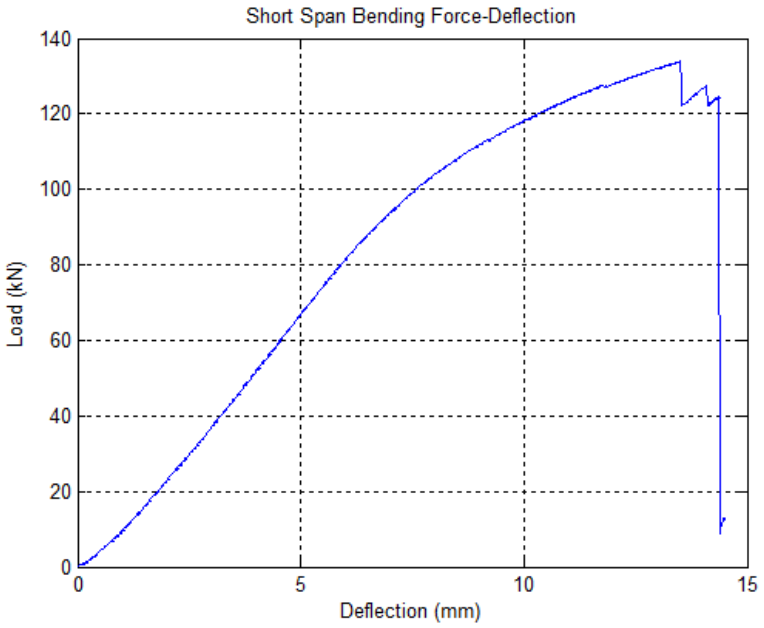

Fig. 6.10. Short span bending test force-deflection (Test 5-1)

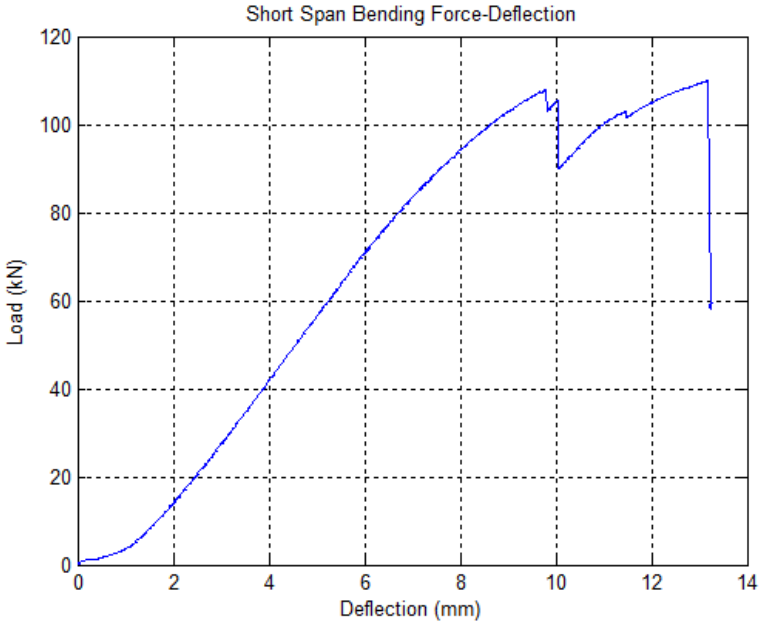

Fig. 6.11. Short span bending test force-deflection (Test 5-2)

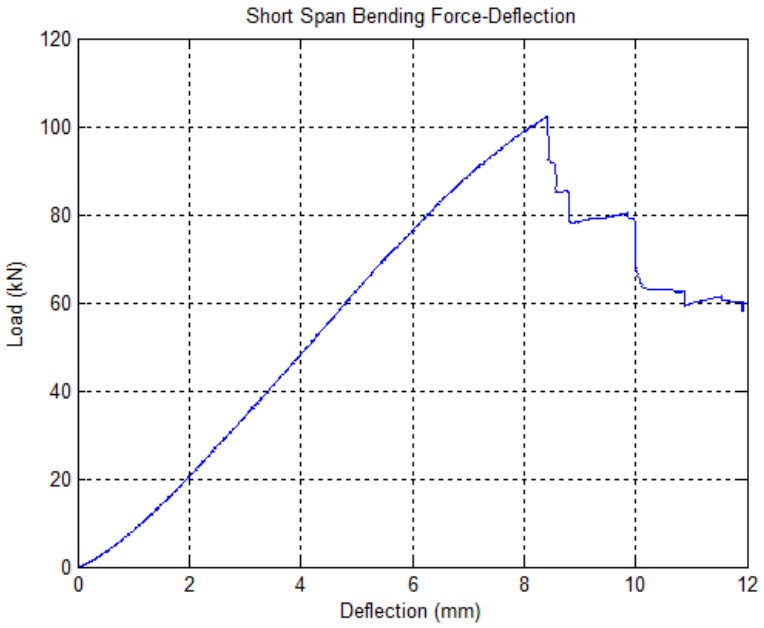

Fig. 6.12. Short span bending test force-deflection (Test 5-3)

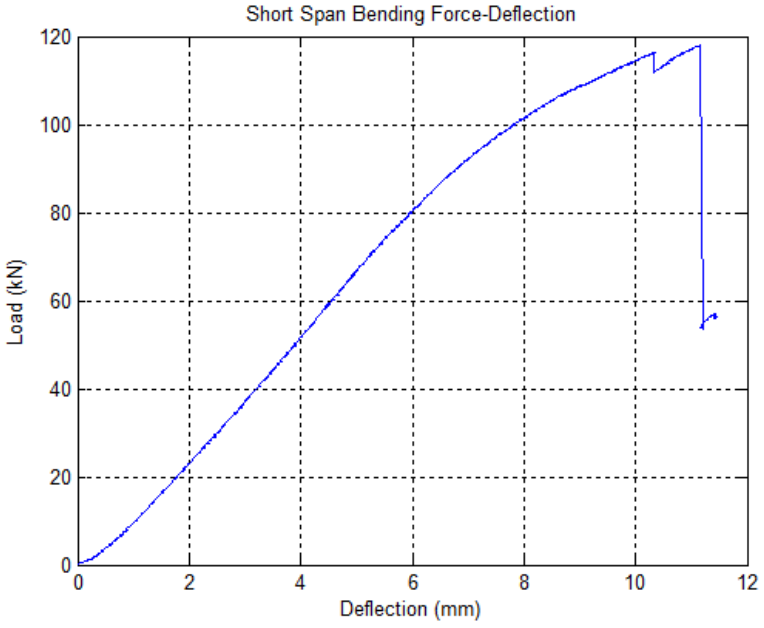

Fig. 6.13. Short span bending test force-deflection (Test 5-4)

6.2 Additional Figures Chapter 3

6.2.1 Panel Tension Test Figures

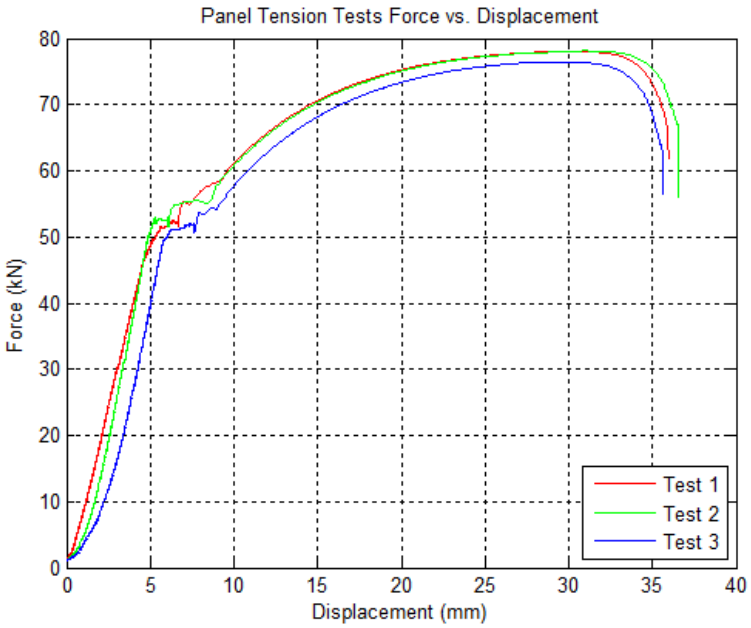

Fig. 6.14. Panel tension tests force-displacement (not adjusted for slack)

6.2.2 Panel Cyclic Test Figures

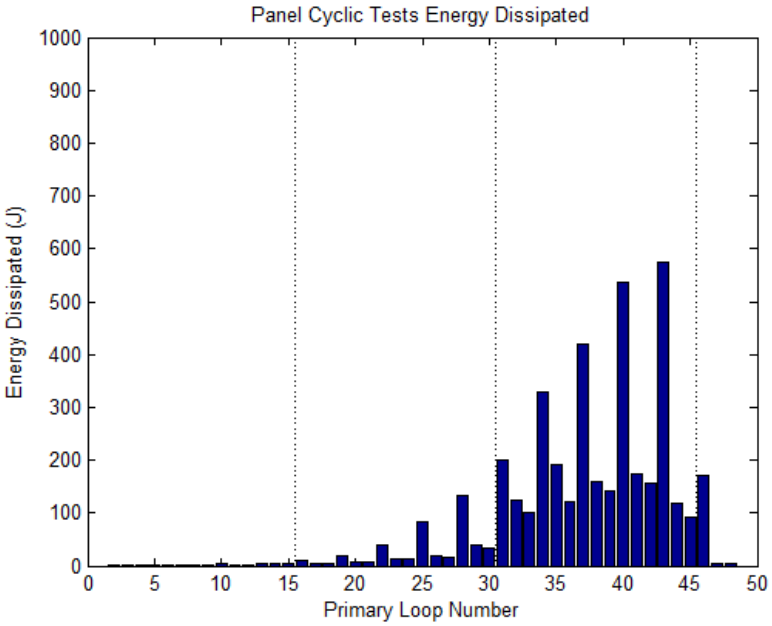

Fig. 6.15. Panel cyclic test energy dissipated (Test 1)

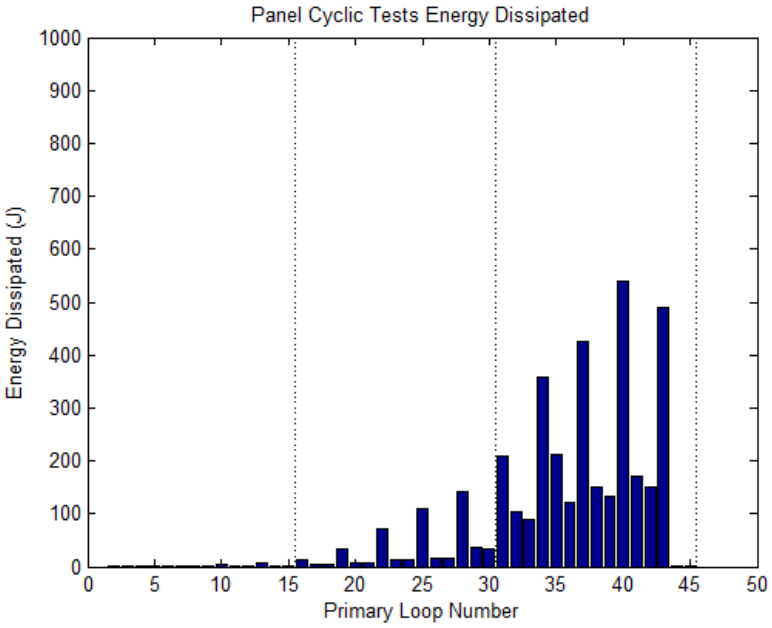

Fig. 6.16. Panel cyclic test energy dissipated (Test 2)

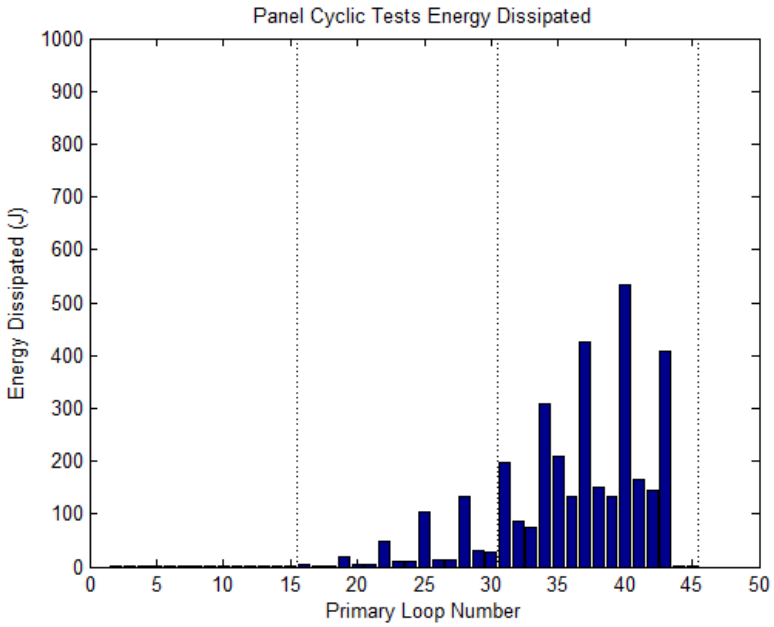

Fig. 6.17. Panel cyclic test energy dissipated (Test 3)

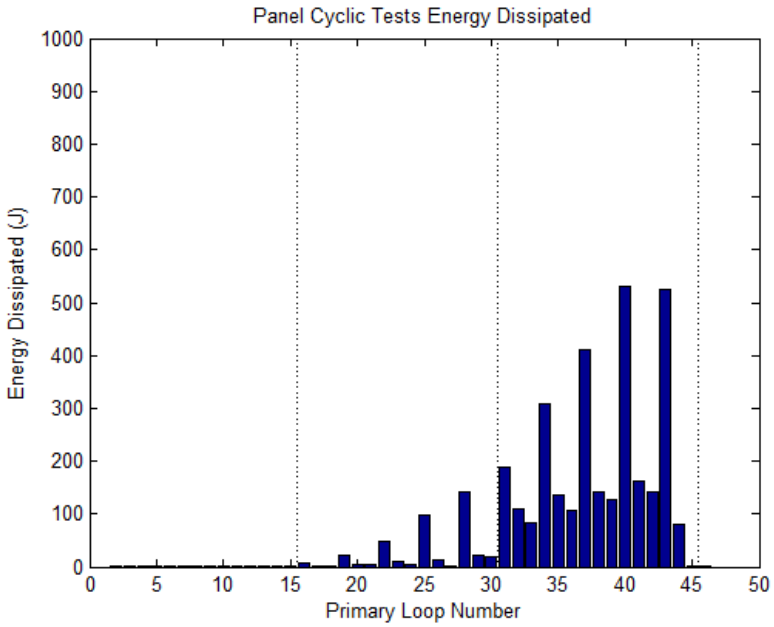

Fig. 6.18. Panel cyclic test energy dissipated (Test 4)

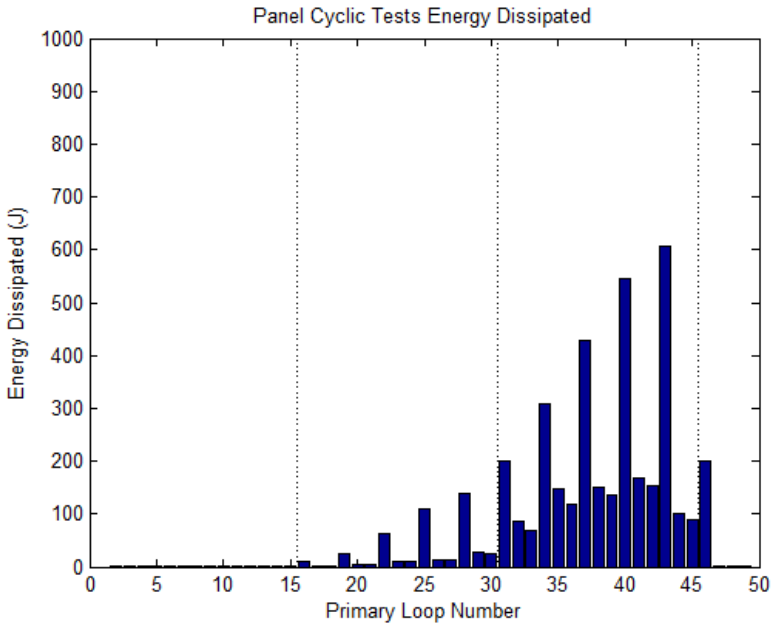

Fig. 6.19. Panel cyclic test energy dissipated (Test 5)

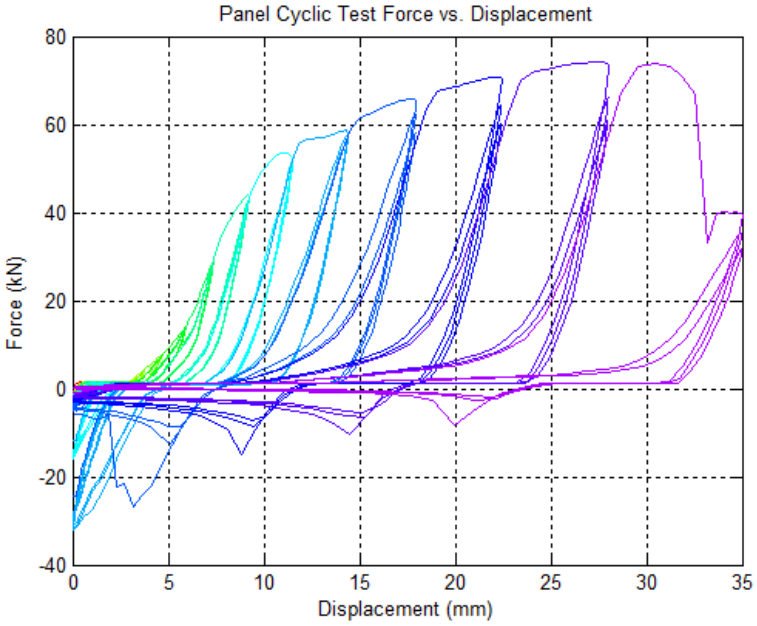

Fig. 6.20. Panel cyclic test force-displacement (Test 1)

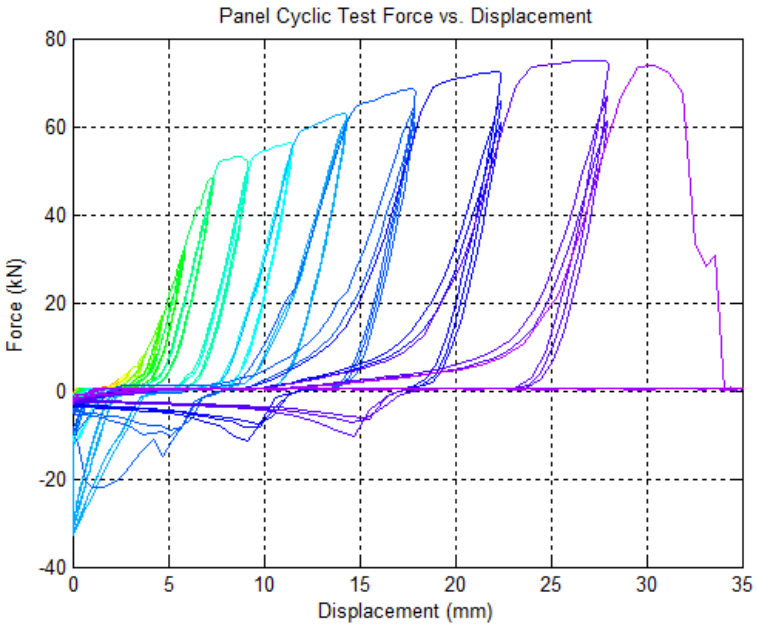

Fig. 6.21. Panel cyclic test force-displacement (Test 2)

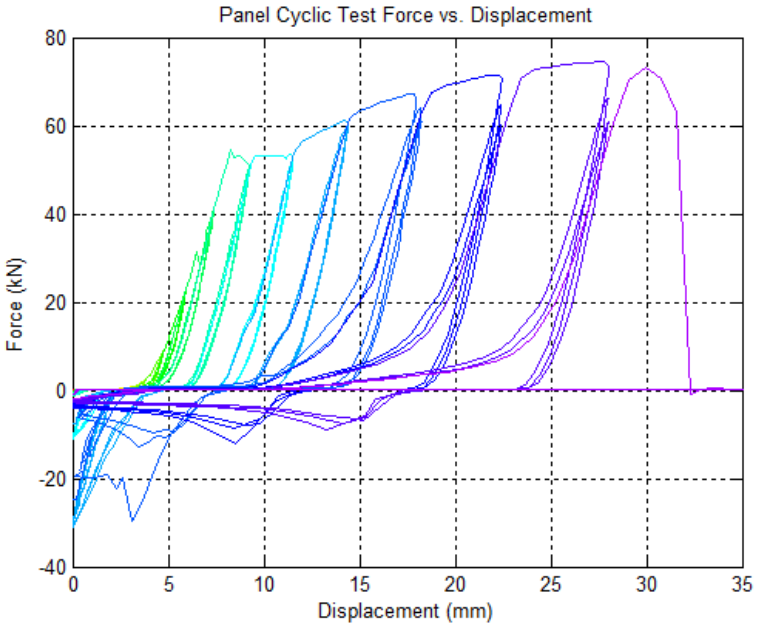

Fig. 6.22. Panel cyclic test force-displacement (Test 3)

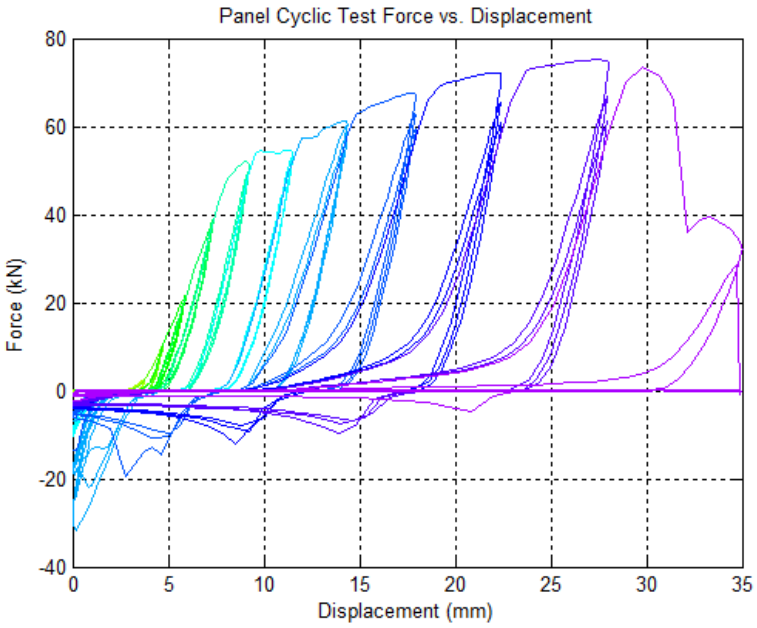

Fig. 6.23. Panel cyclic test force-displacement (Test 4)

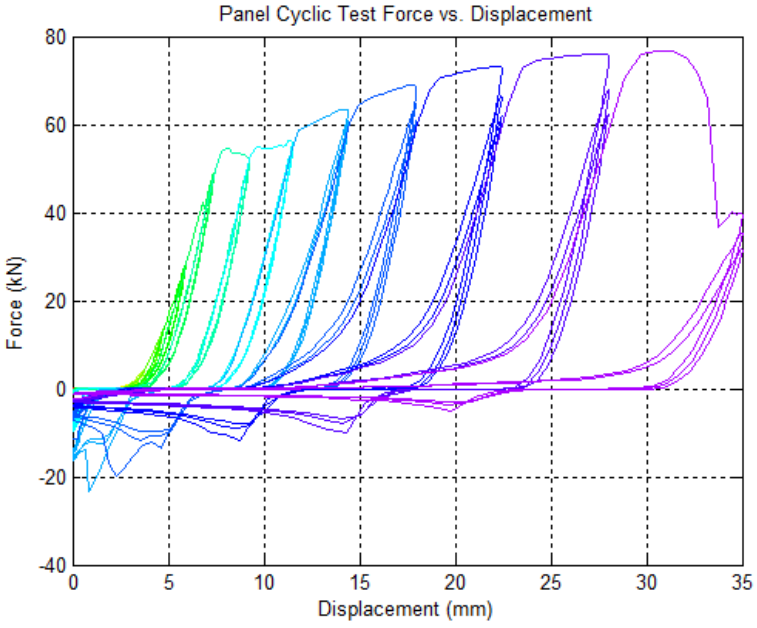

Fig. 6.24. Panel cyclic test force-displacement (Test 5)

6.2.3 Extended Tables Results

Table 6.1. Individual Tension Tests

Test	Force at Ultimate (kN)	Force at Failure (kN)	Disp. at Ultimate (mm)	Disp. at Failure (mm)
1	38.19	26.49	29.59	32.51
2	37.94	26.94	31.11	33.71
3	37.67	25.75	29.86	31.83
St Dev	0.260	0.602	0.812	0.951
Ave	37.932	26.39	30.19	32.68
COV	0.69%	2.28%	2.69%	2.91%

Table 6.2. Panel Tension Test Results

Test	Force at Ultimate (kN)	Force at Failure (kN)	Disp. at Ultimate (mm)	Disp. at Failure (mm)
1	78.06	66.05	29.59	35.94
2	78.13	67.48	31.11	36.45
3	76.43	62.98	29.86	35.56
St Dev	0.964	2.296	0.812	0.446
Ave	77.542	65.50	30.19	35.98
COV	1.24%	3.51%	2.69%	1.24%

Table 6.3. Panel Cyclic Test Results

Test	Initial Slack (mm)	Disp at Ultimate	Adj. Disp. at Ultimate	Disp at Failure	Adj. Disp. at Failure	Energy Dissipated	Force at Ultimate	Force at Failure (kN)
1	2.6924	27.432	24.7396	32.5882	29.8958	4100	74.15	66.99
2	1.7272	27.432	25.7048	31.877	30.1498	3703	75.05	67.53
3	3.4544	27.432	23.9776	31.5595	28.1051	3394	73.16	62.98
4	2.8702	29.718	26.8478	31.4198	28.5496	3472	73.51	66.14
5	2.7432	30.48	27.7368	33.2232	30.48	3975	76.70	65.83
St Dev	0.622	1.485	1.525	0.758	1.045	307	1.42	1.76
Ave	2.697	28.50	25.80	32.13	29.44	3729	74.51	65.90
COV	23.05%	5.21%	5.91%	2.36%	3.55%	8.23%	1.90%	2.67%

6.2.3 Supplemental Design Calculations

Rocking Wall Design (According to Restrepo and Rahman 2007)

Purpose:
1. Attaining a non-linear response by developing separation gaps at the wall bases
2. Ensuring self-centering, even after a large displacement excursion

Control of Sliding Shear

$h_{eff} := 2.438\ m$ $\omega_d := 1.2$ Ratio between static and dynamic coeff of friction $\omega_f := 1.5$

$l_w := 1.219\ m$ $\omega_\kappa := 1.0$ Accounts for increase in shear force from walls of different length $\mu_f := 0.7$ Sliding Friction Coeff

Effective height-to-wall length ratio must be greater to avoid sliding shear

$\frac{h_{eff}}{l_w} = 2 > \frac{\omega_d \cdot \omega_\kappa \cdot \omega_f}{2 \cdot \mu_f} = 1.286$

Control of Prestressing Force

$A_{tp} := 140\ mm^2$ $f_u := 1862\ MPa$ $b_e := 158.8\ mm$

$F_{pp} := 0.9 \cdot f_u \cdot A_{tp} = 234.612\ kN$ $E_{ps} := 196.5\ GPa$

$d_{ps} := 610\ mm$ $c := 610\ mm$ $l_{ps} := 2.438\ m$

$\varepsilon_{ps} := 0.0085$ $\Delta_{ps} := \varepsilon_{ps} \cdot l_{ps} = 20.723\ mm$ $\theta_{ls} := \frac{\Delta_{ps}}{d_{ps}} = 0.034$

Limit state criterion to ensure tendons remain elastic at the life safety performance objective

$F_{po} := F_{pp} - \frac{E_{ps} \cdot A_{tp} \cdot (d_{ps} - c)}{l_{ps}} \cdot \theta_{ls} = 234.612\ kN$ $f_y := 248\ MPa$

$f_{para} := 41.4\ MPa$

$\rho_w := 480\ \frac{kg}{m^3}$ $V_w := h_{eff} \cdot l_w \cdot b_e = 0.472\ m^3$

$f_{su} := 434\ MPa$

$P_u := \rho_w \cdot V_w \cdot 9.81\ \frac{m}{s^2} = 2.222\ kN$ $\varepsilon_{su} := 0.20$

$d_{ed} := 305\ mm$

$A_{sd} := \frac{2}{3}\left(\frac{P_u + F_{po}}{f_y}\right) = 636.651\ mm^2$

Pick steel dissipator area less than the above value (Asd)

$D_{mill} := 9.53\ mm$ $A_{mill} := \frac{\pi \cdot D_{mill}^2}{4} = 71.331\ mm^2$ $A_{sd} := 4 \cdot A_{mill} = 285.322\ mm^2$

$F_{ed} := A_{sd} \cdot f_{su} = 123.83\ kN$

$l_e := \left(\frac{3}{2}\right) \cdot \frac{\theta_{ls}}{\varepsilon_{su}} \left(c - d_{ed}\right) = 77.711\ mm$ $1.5 \cdot l_e = 116.567\ mm$

$P_T := P_u + F_{po} = 236.834\ kN$

Does the force from post-tensioning and dead load overcome the strength of the energy dissipators? $P_T > F_{ed} = 1$

$F_{id} := A_{sd} \cdot f_y = 70.76\ kN$

$F_{pi} := 0.4 \cdot f_u \cdot A_{tp} = 104.272\ kN$

Ratio of prestressing bending resistance contribution, to the dampers bending resistance contribution. Recommended to be between 1.25 and 1.5.

Initial **Ultimate**

$\lambda_i := \frac{F_{pi}}{F_{id}} = 1.474$ $\lambda_u := \frac{F_{pp}}{F_{ed}} = 1.895$

Design is 3/8" diameter energy dissipators and 6/10" diameter 270K prestressing strand

Energy Dissipator Estimates

$f_y := 248\ MPa$ $\quad D_{mid} := 9.525\ mm$ $\quad r_{mid} := \frac{D_{mid}}{2}$

$f_u := 400\ MPa$ $\quad A_{mid} := \frac{\pi \cdot D_{mid}^{2}}{4} = 71.256\ mm^2$

$E := 200\ GPa$

$F_u := f_u \cdot A_{mid} = 28.502\ kN$

$F_{tot} := 2 \cdot F_u = 57.005\ kN$

From Connection Calculations

$F_{bolted} := 248\ kN$ $\quad F_{screw} := 54\ kN$

$F_{conn} := F_{bolted} + F_{screw} = 302\ kN$

Design for Compression

$K := 1.0$ $\quad I_{mid} := \frac{\pi \cdot r_{mid}^{4}}{4} = 404.045\ mm^4$ $\quad r := \sqrt{\frac{I_{mid}}{A_{mid}}} = 2.381\ mm$

$L := 457\ mm$ $\quad L_{tot} := 457\ mm$

$\lambda_p := 0.38 \cdot \sqrt{\frac{E}{f_y}} = 10.791$ $\quad \lambda_r := 0.11 \cdot \frac{E}{f_y} = 88.71$

$\frac{K \cdot L}{r} = 191.916$

Critical Buckling Stress

$f_e := \frac{\pi^2 \cdot E}{\left(\frac{K \cdot L}{r}\right)^2} = 53.593\ MPa$ $\quad f_{cr} := 0.877 \cdot f_e = 47.001\ MPa$

$\varepsilon_{cr} := \frac{f_{cr}}{E} = 0.024\%$ $\quad \Delta_{cr} := \varepsilon_{cr} \cdot L_{tot} = 0.107\ mm$

$F_{cr} := f_{cr} \cdot A_{mid} = 3.349\ kN$

Bolted Connection (According to NDS 2012)

Parameters

$D := 25.4\ mm$ $\quad l_m := 140\ mm$

$F_{yb} := 310\ MPa$ $\quad F_{em} := 38.6\ MPa$

$F_{es} := 600\ MPa$ $\quad K_\theta := 1.25$

$l_s := 25.4\ mm$ $\quad R_e := \frac{F_{em}}{F_{es}}$

Yield Limit Equations
Double Shear

$R_d := 4 \cdot K_\theta$ $\quad Z_{Im} := \frac{D \cdot l_m \cdot F_{em}}{R_d} = 27.452\ kN$ Bearing Failure Mode

$Z_{Is} := \frac{2 \cdot D \cdot l_s \cdot F_{es}}{R_d} = 154.838\ kN$ Shear Failure Mode

$R_d := 3.2 \cdot K_\theta$ $\quad k_3 := -1 + \sqrt{\frac{2 \cdot (1 + R_e)}{R_e} + \frac{2 \cdot F_{yb} \cdot (2 + R_e) \cdot D^2}{3 \cdot F_{em} \cdot l_s^{\,2}}}$

$Z_{IIIs} := \frac{2 \cdot k_3 \cdot D \cdot l_s \cdot F_{em}}{(2 + R_e) \cdot R_d} = 34.042\ kN$ Bending Failure Mode

SOLUTION: Assumption that the wall connection adds enough rigidity so that bending and bearing failures will not control

$C_D := 1.6$

$F_{bolted} := Z_{Is} \cdot C_D = 247.741\ kN$

Structural Fastener Connections (According to NDS 2012)

Parameters

$n := 3$ $D := 6.35\ mm$ $\gamma := 270000 \cdot 0.25^{1.5}\ \frac{lbf}{in}$ $s := 25.4\ mm$

$E_s := 200\ GPa$ $A_s := 1290\ mm^2$ $EsAs := E_s \cdot A_s = (2.58 \cdot 10^5)\ kN$

$E_m := 9\ GPa$ $A_m := 15484\ mm^2$ $EmAm := E_m \cdot A_m = (1.394 \cdot 10^5)\ kN$

$R_{EA} := \frac{EmAm}{EsAs}$ $u := 1 + \gamma \cdot \frac{s}{2} \cdot \left(\frac{1}{EmAm} + \frac{1}{EsAs}\right)$ $m := u - \sqrt{u^2 - 1}$

Group Action Factor

$$C_g := \left(\frac{m \cdot (1 - m^{2n})}{n \cdot \left((1 + R_{EA} \cdot m^n) \cdot (1 + m) - 1 + m^{2n}\right)}\right) \cdot \left(\frac{1 + R_{EA}}{1 - m}\right) = 0.999$$

Structural Fastener Capacity

$Z_{para} := 934\ N$ $n_{screw} := 18$ $C_D := 1.6$

$F := 2 \cdot Z_{para} \cdot n_{screw} \cdot C_D = 53.798\ kN$